Cored and Low Density Halos

A *Magneticum* Simulation's Standpoint on Relations Between Flat Inner Dark Matter Distributions, Low Dark Matter Density and Their Evolution

Bachelor thesis at the Faculty of Physics
Ludwig-Maximilians-University Munich

Submitted by
Sebastian Jonas Langer

Supervised by
Dr. habil. Klaus Dolag

Munich, July 24, 2020

Flache und wenig dichte Halos

Relationen zwischen im inneren flachen und wenig dichten Halos und deren Entwicklung in der *Magneticum* Simulation

Bachelorarbeit an der Fakultät für Physik
Ludwig-Maximilians-Universität München

Eingereicht von
Sebastian Jonas Langer

Betreut von
Dr. habil. Klaus Dolag

München, den 24.07.2020

Contents

1. Introduction

How can we discover something that we cannot see? This question points to a recurring problem in physics, from the smallest particles to cosmological scales, from electrons to dark matter and dark energy. Scientists have been inventing better and more innovative ways to prove the existence of the invisible. To discover the most fundamental particles of our universe, powerful accelerators and detectors have been developed. To prove the existence of dark matter it took great observational instruments and a physicist's best tool: mathematics.

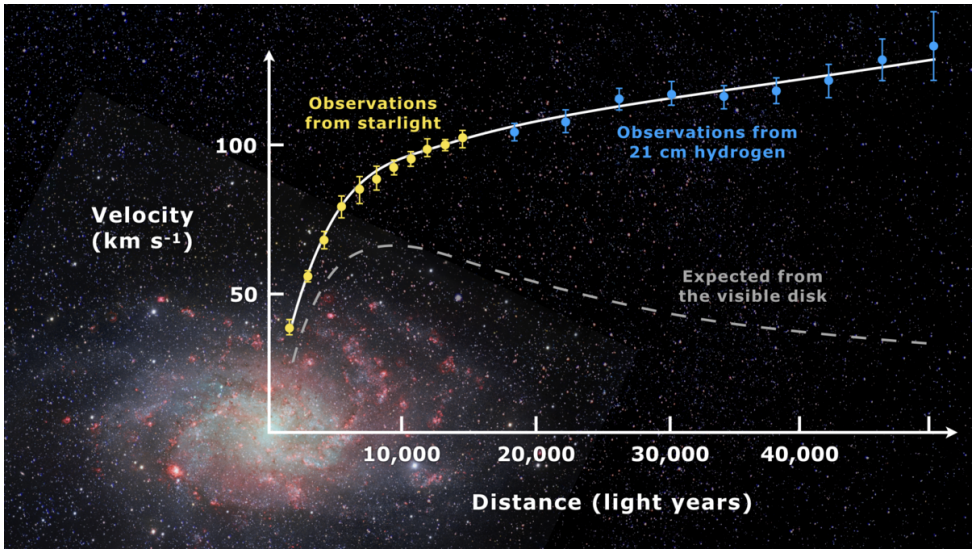

Figure 1.1.: Rotational velocity as a function of the radius from the center of the spiral galaxy Messier 33. Observations from star light and gas (yellow and blue) do not agree with calculations without dark matter (grey). The real velocity curve is rising and exceeds the theoretical values (source: en.wikipedia.org/wiki/Galaxy_rotation_curve).

The most important indicator for dark matter are the rotation curves of galaxies. They give the circular velocity of an object at a given radius from the center. Already in 1922, Kapteyn spoke of dark matter in his work on the properties of the Milky Way. If one assumes a perfect circular rotation, then gravitational and centripetal force on a mass point must be equal:

$$F_c = F_G \Rightarrow \frac{m \cdot v^2}{r} = G\frac{m \cdot M(r)}{r^2} \Rightarrow v(r) = \sqrt{G\frac{M(r)}{r}} \tag{1.1}$$

We have found a relation between the rotational velocity, the radius and the total mass

enclosed within it.
Astronomers have measured the real rotational velocities of stars and gas inside a galaxy. What they found contradicted what calculations based only on visible matter would predict. Zwicky (1933) concluded that a dark matter mass of 400 times the luminous matter would be needed to explain rotational velocities in galaxies of the Coma Cluster.

This paradigm also becomes obvious in figure 1.1, in which observational data from stars and gas from the spiral galaxy Messier 33 is depicted. The actual rotational velocities (blue and yellow) are much higher - especially in the outer part of the galaxy - than one would expect from the visible mass and equation 1.1 (dotted line). Thus the enclosed mass within these radii must be greater than what is visible from stars and gas. There has to be something that is interacting gravitationally, but not in any other way: dark matter.
Twenty-seven percent of our universe consists of this strange dark matter and sixty-eight percent of dark energy[1]. Dark energy is responsible for the expansion of the universe against the gravitational pull of matter. This concept of an expanding universe was deemed unthinkable at first. Even the cosmological constant was originally introduced by Einstein, only so that his theory of general relativity would render a static universe as a solution, not an expanding one (Mo et al., 2010). But in 1929 Edwin Hubble proved that the velocity at which galaxies are moving away from us is proportional to their distance to us[2]. This would only be possible in an expanding universe. So all doubts were eradicated and even Einstein called his previous disbelief "the biggest blunder of [his] life"(Mo et al., 2010, p.16). This creation of space occurs not at the edge of the universe, but simultaneously at every point in space. Thus it should be imagined as a raisin bread baking in the oven, in which the distance between every raisin grows continuously.
This expansion effects the light that is coming to us from other galaxies. On its way, the space within the wave itself expands. Thus the further away we look, the more the light has shifted towards larger wavelengths[1]. This is called *redshift* and is an alternative way of describing the amount of time light has travelled.
So apparently we can neither grasp nor see these dark components, but scientific research dictates their existence. That means that everything we know, everything that is made up of atoms, from small particles to stars and galaxies sums up to only five percent of the universe[1]. This is all the more reason to study and try to comprehend more about dark energy and dark matter. The aim of this work is to present and form conclusions from simulation data of the dark matter distribution in galaxies and beyond.

[1] science.nasa.gov/astrophysics/focus-areas/what-is-dark-energy
[2] www.scientificamerican.com/article/the-evolution-of-the-universe/

2. The Evolution of the Universe

Let us take a quick look at the evolution of the universe, from big bang to today. For having a complete picture of the topics discussed in this work, it is very useful to be aware of the timeline before and after the first cosmological structures formed.

2.1. The Λ-CDM Model

The most common theory of the big bang is the Λ-CDM (Lambda cold dark matter) model. It assumes that dark energy is responsible for the expansion of space, which is associated with the Lambda constant[1].
Cold dark matter means that the kinetic energy of the dark matter is comparably low, making it non-relativistic (Brouwer et al., 2017). To date, no such thing as a dark matter particle has been experimentally found. Assuming its existence one could imagine dark matter as a gas-like but collisionless and dissipationless cloud of particles, similar to how dark matter is treated in the simulations.
The Lambda-CDM model has been very successful at explaining the universe and its properties from big bang untill today.

2.2. The Big Bang

Roughly 13.7 billion years ago, at the big bang, the whole universe was compressed into an extremely dense, hot and small volume of only a few cubic millimeters[2]. The universe was so small that it was affected by quantum effects. As suspected by Mukhanov and Chibisov in 1981 and later confirmed by observations of the European Space Agency in 2015 (Mukhanov, 2016), quantum fluctuations gave rise to the inhomogeneity in the universe without which not a single galaxy could have formed. Even the four fundamental forces of physics (strong and weak, electromagnetic and gravitational force) were indistinguishable from each other at this point (Georgi & Glashow, 1974). Within 10 seconds after the big bang only photons, leptons and quarks propagated through space[3]. Thereafter protons and neutrons existed and formed the first atomic nuclei[4]. During this phase the universe was expanding extremely fast, doubling its size not less than 90 times[2].

[1] en.wikipedia.org/wiki/Lambda-CDM_model
[2] www.space.com/13320-big-bang-universe-10-steps-explainer.html
[3] en.wikipedia.org/wiki/Universe#Chronology_and_the_Big_Bang
[4] www.scientificamerican.com/article/the-evolution-of-the-universe/

2.3. Early Universe

For the first 370 thousand years the universe was so hot that is was like a plasma, making it nontransparent for light[5]. When the universe had cooled enough, electrons could bind to these nuclei. Thus the first neutral atoms (mostly hydrogen, but also helium and traces of lithium) were created (Mo et al., 2010, p.17) and light was no longer scattered. The afterglow from exactly this recombination period is what astronomers call the *cosmic microwave background*.

2.4. Galaxy formation

Roughly 400 million years after the big bang, the universe's evolution is less action packed. Because of the initial inhomogeneities there are regions in which gas is denser. These gas clouds collapse due to the gravitational pull and form the first stars and galaxies. Some of those stars are even part of an early milky way galaxy[6], making it almost as old as the universe itself. Since the gas clouds retain their inner angular momentum while collapsing many evolve to rotating flat disk galaxies. Like the milky way these disk galaxies often arrange their stars in spiral arms. Other galaxies become ellipticals, which are 'egg-shaped' and dispersion dominated (Teklu et al., 2015) giving it less structure than disk galaxies. Galaxies can grow through mergers in which two or more galaxies come close enough to bind to each other and eventually combine. This happens mainly at higher redshifts - meaning the more distant past - since the distance between two unbound objects increases steadily due to the expansion.
Over time, cycles of gas accretion, star formation, supernovae and gas expulsion repeat inside the galaxies. Through fusion in the stars and supernovae heavier elements are created.
In cosmological simulations such as the one used in this work, one tries to reenact all these processes to gain a better understanding of our universe and galaxy formation.

[5] www.space.com/13320-big-bang-universe-10-steps-explainer.html
[6] www.spiegel.de/wissenschaft/weltall/13-6-milliarden-jahre-milchstrasse-ist-fast-so-alt-wie-das-universum-a-313697.html

3. Cold Dark Matter Halos

Dark matter halos are an important part of this work. Roughly at the beginning of the galaxy formation phase described in the previous section, halos start to be the predominant part of cosmological structures. Halos are regions extending far beyond the size of the galaxies enclosed in them. One uses the definition of a halo to include the dark matter that is present in and around the galaxy and to be able to compare different halos and galaxies to each other.
The distribution of dark matter is approximately spherical. Of course, the dark matter distribution does not have an instant cut, but is smooth. One defines the radius of such a halo as the radius in which the enclosed density is 200 times the critical density of the universe (Navarro, Frenk, & White, 1996). This critical density is the mean density of the universe, which would be required to bring the expansion of the universe to a halt (after an infinite amount of time)[1].
Dark matter may only interact with matter through gravitation, which does not mean that physical interactions between baryonic matter is irrelevant when examining dark matter. This is best seen in Dutton et al. (2016), where the dark matter distribution can either be expanded or contracted by baryonic dynamics, depending on the star formation rate of the galaxy.

A widely used formula to describe the density distribution of cold dark matter in halos is the NFW-profile, introduced by Navarro et al. in 1996:

$$\rho_{NFW}(r) = \frac{\rho_0}{\frac{r}{r_s} \cdot (1 + \frac{r}{r_s})^2} \tag{3.1}$$

Where ρ_0 and the scale radius r_s are parameters of the fit. If one examines the NFW-profile for small radii, one can see that the first order term dominates and the density approximately follows a power law:

$$\rho_{NFW}(r) = \frac{\rho_0}{\frac{r}{r_s} + 2 \cdot \frac{r^2}{r_s^2} + \frac{r^3}{r_s^3}} \xrightarrow[r \longrightarrow 0]{} r_s \cdot \rho_0 \cdot r^{-1} \tag{3.2}$$

A perfect NFW density distribution thus has an exponent of -1 for its inner radii, also called the (inner) slope. An interesting feature of some halos is a very flat inner density distribution, named *core* (Dekel et al., 2017), which of course relates to a less negative inner slope. The opposite - an unusually steep distribution - is called *cusp*.

[1] www.astronomy.swin.edu.au/cosmos/C/Critical+Density

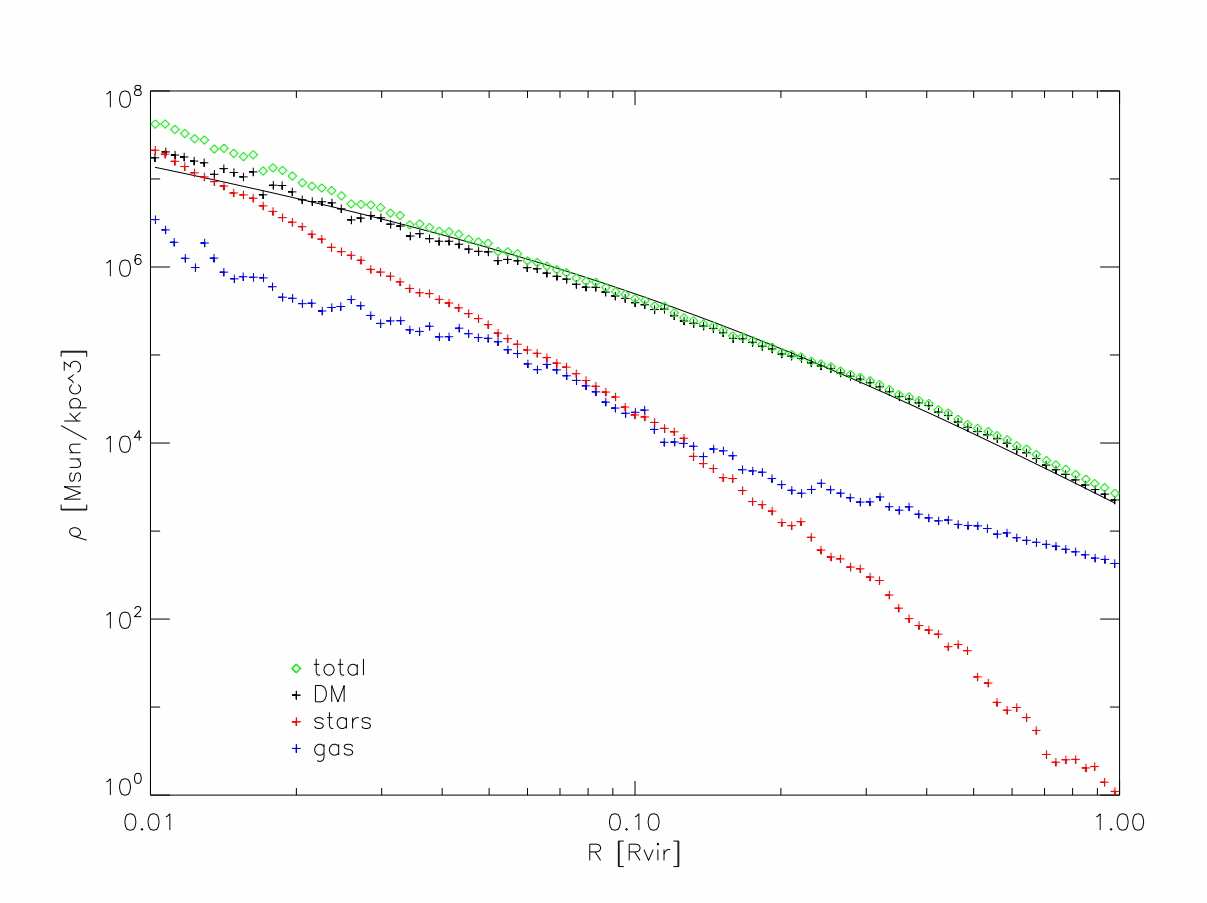

Figure 3.1.: Exemplary density distribution of dark matter, gas, stars and all three (total) within the virial radius of halo 50. The dark matter distribution is well fitted with the NFW-profile (black line). Dark matter dominates at most radii. The stellar component is concentrated within ten percent of the virial radius.

Figure 3.1 is an exemplary plot for the dark matter density and other components from the center to the virial radius. The depicted galaxy has a stellar mass of $2.7 \cdot 10^{11} M_\odot$ and a halo mass of $7.6 \cdot 10^{12} M_\odot$. One can observe that the total density is mostly dominated by the dark matter. Only in the inner two percent of the virial radius stars contribute a comparable mass. In accordance with most halos the majority of the stellar population resides within ten percent of the virial radius. When speaking of a galaxy one usually refers to this inner star-dense and luminous part. While the gaseous component is less dense at small radii, it outweighs the stars in the outer part. A fraction of the gas often has a relatively high kinetic energy (temperature) giving it a larger radius.
The dark matter density distribution is well-fitted with the NFW profile (black line), which has the parameters $\rho_0 = 1.3 \cdot 10^6 M_\odot/\mathrm{kpc}^3$, $r_s = 69.4$ kpc $= 0.12 \cdot R_{vir}$ and concentration parameter $c = R_{vir}/r_s = 8.1$.
In this work I will analyse different properties of dark matter halos and shine a light on the evolution of these parameters throughout the formation history of the galaxies.

4. Simulation and Methods

Scientists try to reproduce the dynamics and structures of our universe with simulations. I will give information on the simulation that was used for this work and discuss the methods I applied to evaluate the simulation's output data.

4.1. Magneticum Simulation

The data used in this work stems from *Magneticum Pathfinder*, a set of hydrodynamical simulations which replicate the evolution of cosmological structures on various scales. Large scale simulations provide insight into big structures such as the cosmic web. On a relatively smaller scale simulations can act as a counterpart to observed galaxy and halo properties.
The Magneticum simulation is based on the N-body/SPH(Smoothed Particle Hydrodynamics) code GADGET-3 (see Dolag et al., 2005; Donnert et al., 2013; Beck et al., 2016). This allows for gas cooling and thermal conduction (Jubelgas et al., 2004). Kinetic feedback from stellar winds is modeled proportionally to the star formation rate (SFR) and according to Springel and Hernquist (2003). Chemical enrichment thorough supernovae and AGB (asymptotic giant branch) stars (Tornatore et al., 2007) and the radiative cooling thereof (Wiersma et al., 2009) is accounted for as well.
Furthermore Magneticum is able to simulate black hole growth and their AGN (active galactic nucleus) feedback (see Springel et al., 2005; Di Matteo et al., 2005; Fabjan et al., 2010). Black holes are able to grow in mass by accreting surrounding gas or merging with other black holes. At the same time AGN feedback creates outflows of gas, which can suppress star formation and deposit energy within its surrounding. Even magnetic fields in galaxy clusters are implemented in Magneticum (Dolag & Stasyszyn, 2009).
These physical processes are not only crucial for accurately simulating galaxies, but also for the dark matter halos, since baryons influence dark matter as previously mentioned.
Cosmological constants are set according to the Wilkinson Microwave Anisotropy Probe (Larson et al., 2011). The Hubble constant is $H_0 = 70.4$, the primordial power spectrum and its normalization are n=0.963 and $\sigma_8 = 0.809$. The cosmological constant Λ_0 is 0.728 and the total matter density Ω_0 is determined as 0.272. The data for this work was taken from *box4* of Magneticum which has a size of 48 Mpc/h and $2 \cdot 576^3$ particles.
What sets Magneticum apart from other simulations is for example the treatment of the initial mass function. It describes the distribution of mass for a given population of stars at a given time[1]. Magneticum is not tuned to perfectly fulfill this function, but rather

[1] en.wikipedia.org/wiki/Initial_mass_function

focuses on accurately treating hot-gas physics without constraining it. Furthermore Magneticum allows for black holes to be moved from the galaxy center during, for example merger events, when other simulations fix the position in the center. This can lead to important differences in output data and maybe even allows Magneticum to produce the interesting data that I will discuss in the following sections.
For more details and information about the simulation also see the Magneticum website[2].

4.2. Fitting Methods for the Inner Halo

The raw data from the simulation has to be analyzed and visualized. Only then can one form conclusions. I will now describe the methods with which I have been working.
One of the most relevant parameters for this work is the inner slope which I already mentioned and which will later be explained in more detail. To extract it from the data, one must fit a power law to the inner dark matter density of a halo (see eq.3.2). Since I fit this power law only from one to two percent of the virial radius I need an adjusted power law that allows for an offset. One uses the virial radius as reference length to be able to compare halos to each other, even tough they have different sizes.
The bottom row of figure 4.1 contains these fits to data of halo 3 (left) and halo 433 (middle and right). Magneticum's halos are ordered by mass, thus halo 3 is the third heaviest halo et cetera. The parameters shown in the bottom plots relate to this function:

$$\rho_{DM}(r) = \mathrm{A} \cdot r^{B} + \mathrm{C} \tag{4.1}$$

The most important parameter is B which equals the inner slope. The fit works well with the data for halo 3. If one takes a look at the bottom middle and right plot the fit becomes more problematic. The average number of dark matter particles within one bin is much less now, compared to the previous plot. This causes a larger error for the density values and we see more runaways like the data point second from the right. Both plots show halo 433, once with 5 radial bins and once with 6. But the inner slope changes from -0.26 to -1.26 even though we are examining the same halo. Thus the fit and its parameters seem to be very unreliable.

This problem occurred with multiple halos so I changed my approach. I fitted a linear function to the logarithmic density and radius values in accordance with Macciò, Crespi, Blank, and Kang (2020). If we apply the logarithm to equation 3.2 we get:

$$\log(\rho_{NFW}(\mathrm{r})) = \log(\mathrm{r_s} \cdot \rho_0 \cdot \mathrm{r}^{-1}) = -1 \cdot \log\,(\mathrm{r}) + \log(\mathrm{r_s} \cdot \rho_0) \tag{4.2}$$

Again, the NFW slope is -1, but we want to keep this parameter free for the fit. I created logarithmic radial bins so that the values will be equally distributed in the upper plots of figure 4.1. Then the density within these bins and their logarithmic value was calculated.

[2] www.magneticum.org

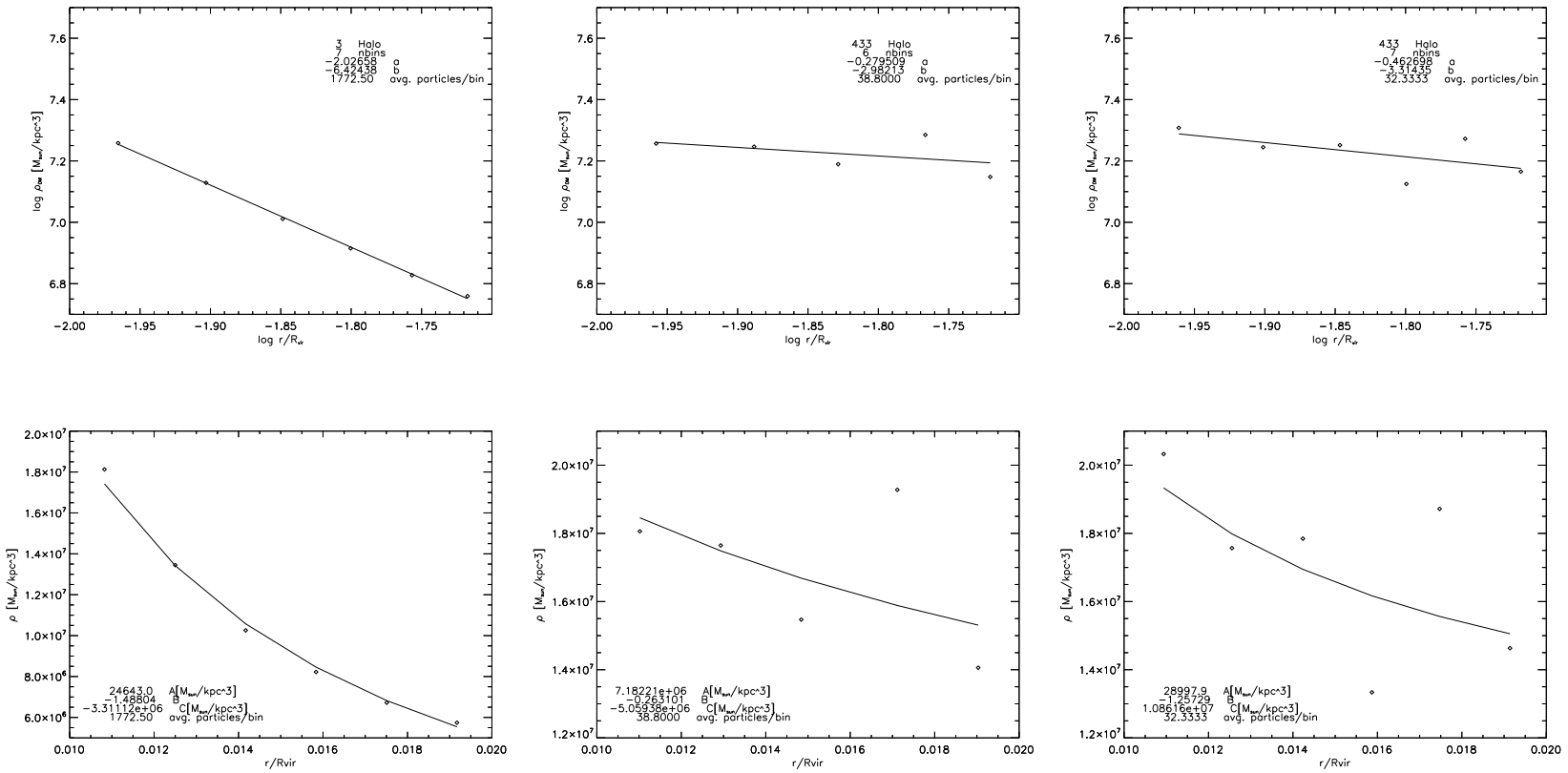

Figure 4.1.: Plots depicting the logarithmic DM density (top row) and DM density (bottom row) within 1-2% of the virial radius. The x-axis gives $\log(r/R_{vir})$ and r/R_{vir} respectively. Keep in mind that the y-axis of the bottom row changes. To gain the inner slope value the top plots are fitted with a two parameter linear function (see eq. 4.3). The bottom row is fitted with a three parameter power law with offset (see eq. 4.1). The left side shows halo 3 with 6 radial bins, the middle shows halo 433 with 5 bins and the right side depicts halo 433 but with 6 bins. The linear fitting yields more consistent parameters when using different bin numbers. It also reflects better on the *steepness* and *flatness* of halo 3 and halo 433 respectively.

By using log (r) and log (ρ_{NFW}(r)) as x- and y-axis one can fit:

$$y = a \cdot x + b \tag{4.3}$$

to the plot. There are now only two free parameters and a is the slope. The linear fit to halo 3 with 6 bins - just like in the plot under it - looks very good. Despite this the slope values between the two techniques disagree by roughly 0.5. The bottom fit seems to slightly underestimate the first and last data point, which would explain the less negative slope.
The linear fits for halo 433 in figure 4.1 are more consistent than the bottom ones. Their slope parameter changes much less (-0.28 to -0.46) when changing the bin number from 5 to 6. All three of the upper plots have the same y-axis range. One can clearly see that the linear fits distinguish much better between the *steepness* and *flatness* of halo 3 and halo 433 respectively.
During my work I looked at many more fits of both methods. Generally, the linear method reflected the density distribution better and was more consistent with changes of the bin number. Thus I continued only with this method. Both are not perfect of course and data from simulations will never deliver values that fit perfectly on the theoretical approach, but neither does nature. A fit should have as many data points available as possible, but at the same time this reduces the particle number within each bin and increases statistical error. As an attempt to compromise between these aspects and to check the consistency of the values I often used the average of multiple fits with different bin numbers. More detailed descriptions of these calculations are found in the respective sections and the appendix.

5. Data Evaluation at Redshift Zero

In the following I will show and explain data and plots created from the Magneticum data at redshift zero. The sample taken from the simulation includes 469 halos, which will forth be depicted as black dots in the plots. For information on the selection criteria for the sample see the appendix. Keep in mind that all elements (gas, stars and dark matter) from subhalos inside the respective halos have not been included in the data. This is common practice and ensures that the various halos are comparable and the disturbances through subhalo structures are compensated for. Subhalo structures are identified by Magneticum's *SubFind*.

5.1. The Inner Slope

An interesting parameter of dark matter halos is the inner slope also denoted as α. I gain the inner slope value from fits to the log ρ - log r plane, as described in section 4.2. From this value one can assess the presence of a cored or cuspy dark matter density distribution (see equation 3.2).
This inner slope is plotted against the stellar mass for each halo in figure 5.1. The data ranges from roughly $6 \cdot 10^9$ to $2 \cdot 10^{11}$ solar masses. Even though there is a wide range of alpha values the green $\alpha(\mathrm{M_{star}})$-function from Macciò et al. (2020) lies within the Magneticum data. They derived their curve from data of the NIHAO-simulations. This general agreement is reassuring and some deviations from the Macciò et al. (2020) data are expected due to different tuning in their simulations. If one looks at figure 2 from Macciò et al. (2020, p.4), they do produce halos that are very steep. Many data points lie way below the expected value of -1 for a perfect NFW-profile, just like the Magneticum data. But only five halos from the same mass range as Magneticum yield inner slopes that tend to be flat. For those with black hole feedback it is only two. Genzel et al. (2020, p.20) even state, that "[...]the results of the currently highest resolution, zoom-in cosmological hydro-simulations (such as Illustris-TNG50/100: Lovell et al. 2018, Pillepich et al. 2019, Nelson et al. 2019) [...] do not predict the 'cored' dark matter distributions". This is where Magneticum stands out as it does clearly produce several high-mass halos with an inner slope significantly higher than -1. To be able to examine more characteristics, halos from figure 5.1 with an inner slope less negative than -0.6 (15 piece) will forth be labeled as *flat* halos. Those more negative than -2 will be labeled *steep* halos. Mind you that the magenta points will not be included in these samples. They were added to the original sample retrospectively and will be discussed later. Plots of the log ρ_{DM}- log r fits and a discussion on the issues of sampling and fitting are found in the appendix.
One can also compare the Magneticum data to observations. Genzel et al. (2020) analysed

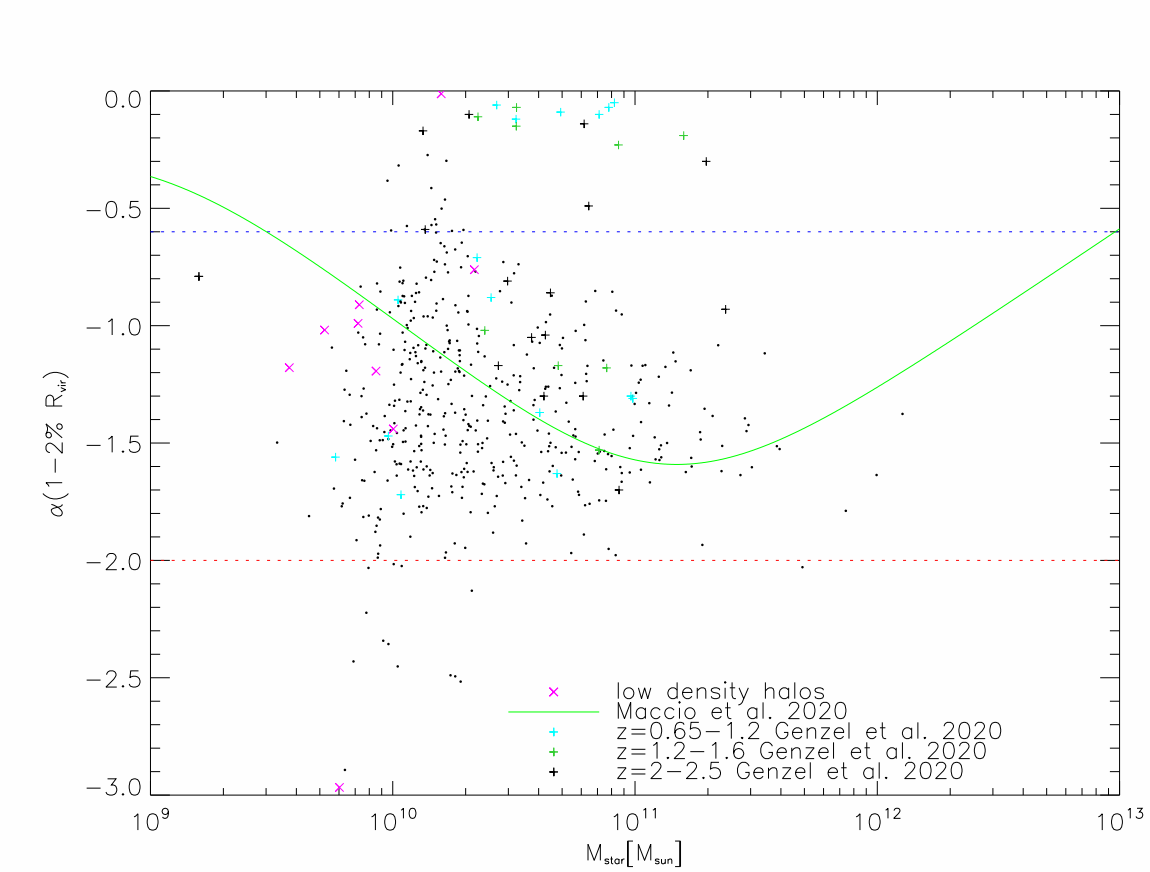

Figure 5.1.: The inner slope plotted against the stellar mass within R_{vir}. Magneticum data is shown as black dots. Halos above the blue line will forth be labeled *flat* halos, those below the red line *steep* halos (magenta points excluded). Magneticum data roughly agrees with the green $\alpha(M_{star})$-function derived from simulation data by Maccio et al. (2020). Also included is observational data from Genzel et al. (2020) with 41 halos in three different redshift categories. Their redshift bin closest to zero covers a similar area than my data. The magenta data points are selected from figure 5.3 and belong to halos that were not included in the original sample.

rotation curves and inferred multiple halo parameters for a sample of 41 disk galaxies. Even though I did not differentiate between spirals or ellipticals, the observations nearest to redshift zero (z=0.65 to z=1.2) cover roughly the same area of stellar mass and inner slope values.
However, there are no observations with a very steep slope, like we see from the simulation. Furthermore Magneticum's flat halos are distributed continuously on the y-axis and on a mass scale of $1 \cdot 10^{10} M_\odot$ to $2 \cdot 10^{10} M_\odot$. Genzel et al. (2020) find flat halos as well, but at slightly higher masses. The distribution on the y-axis seems to be discontinuous, with many halos having a slope near zero. One possible explanation of this might be the fitting method of Genzel et al. (2020). They derive the inner slope from fitting the whole halo

to a slightly altered density profile than equation 3.1 (Genzel et al., 2020, eq.A2, p.24). The least-squares fit will be barely influenced by small changes in the inner region and only adjust the α-parameter if there is a significant change to the -1 slope of the NFW.
What will have to be further examined is why Magneticum's flat halos center around a mass of $1 \cdot 10^{10} M_{\odot}$, whereas those of Genzel et al. (2020) range from $1 \cdot 10^{10} M_{\odot}$ to $2 \cdot 10^{11} M_{\odot}$.
There are multiple physical processes that can contribute to the formation of a cored center. Gas interacting gravitationally with dark matter can affect it in two ways. Adiabatic cooling of gas pulls dark matter to the inside (Dutton et al., 2016). At the same time gas clumps can be decelerated by dynamical friction and transfer energy to dark matter particles, which would then cross over to larger radii (Pontzen & Governato, 2014; Cole, Dehnen, & Wilkinson, 2011). Stellar winds, supernovae and AGN feedback can create (cyclic) gas outflows, which cause dark matter expansion as well. For this to be significant the local gas fraction has to be $\geq$0.1 (Dutton et al., 2016). Furthermore supernovae and AGNs can cause oscillations in the gravitational potential and transfer energy to dark matter particles (Pontzen & Governato, 2012). The displacement of black holes from the center of a galaxy, which Magneticum allows for, would be another source of an oscillation of the potential.
In summary Magneticum does produce cored dark matter distributions, while generally agreeing with observations and the NIHAO simulations.

5.2. The Concentration Parameter

The next parameter to be analysed in my sample is the concentration parameter c. It is defined as the quotient of the virial radius and the scale radius of the NFW-fit (Navarro et al., 1996). The scale radius marks the point at which the fit has a logarithmic slope of -2. Inside of this the slope is flatter, while showing a slope of -3 towards the outside (see eq. 3.2). The Magneticum values in figure 5.2 have roughly the same y-range as the values that Navarro et al. (1996) found in their original paper. One can also see the decrease of c with increasing stellar mass similar to the correlation found for c and the virial mass by Mandelbaum, Seljak, and Hirata (2008).
Do the respective halo samples show a bias in the concentration parameter plot? One would presume the flat halos to be expanded on the inside. Since they presumably deposited dark matter from their center outwards to form the core, the point at which the NFW has a slope of -2 should have increased. The scale radius would consequently be larger and the concentration parameter smaller. Vice versa a steep halo should show a smaller scale radius and larger concentration parameter.

Surprisingly flat and steep halos in figure 5.2 do not show a clear tendency in their concentration parameter, but rather spread widely on the y-axis. On a more detailed note flat halos even populate higher c values, with an average of c=13.0, while steep halos average c=11.0. The physics behind these correlations or rather missing correlations is obviously not yet fully understood, assuming the simulation is correct.

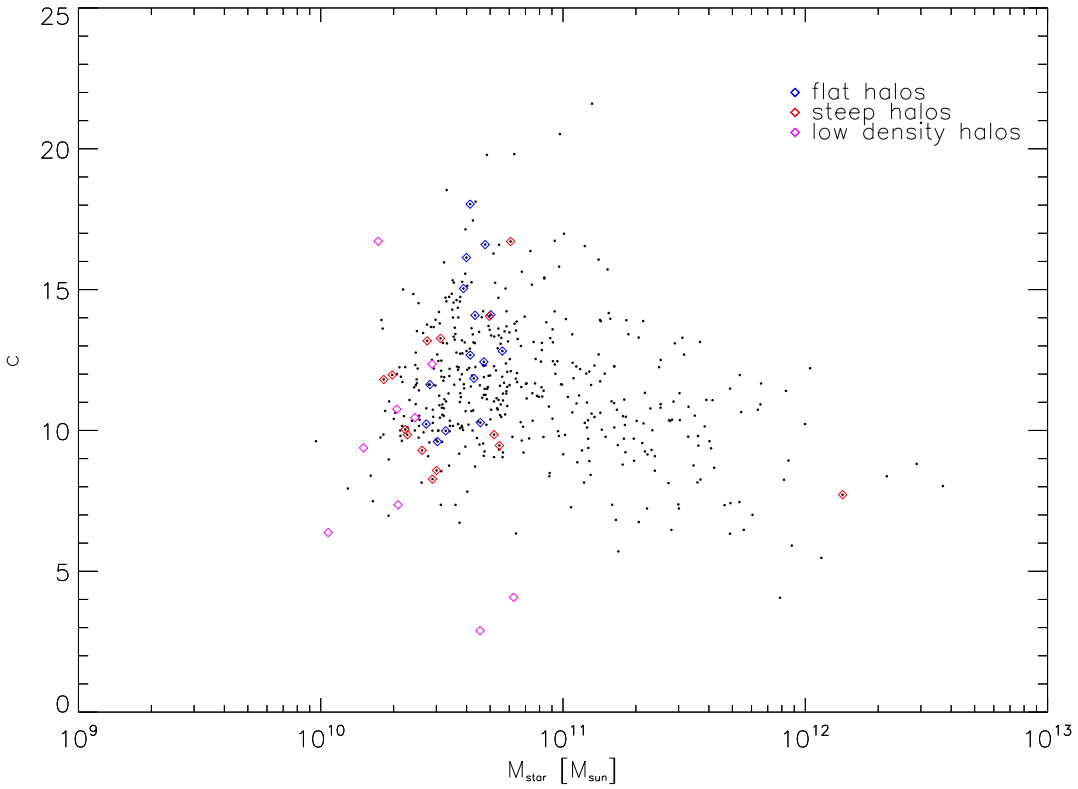

Figure 5.2.: Concentration parameter c from fitting the NFW to Magneticum data plotted against the stellar mass. The range of the values agrees with the data from the original paper by Navarro et al. (1996). Blue and red symbols mark the flat and steep halos categorized in figure 5.1. Unexpectedly their flat or steep slopes do not seem to have significant influence of the concentration of the halo. The magenta data is of halos with low dark matter surface density defined from figure 5.3 and was not included in the original sample of 469 halos. They show a tendency towards lower concentration. This might originate from dark matter being removed from their center. All three colored samples are at the lower end of stellar mass.

A different reason for this disagreement between expectation and simulation might simply be the same as for why the Genzel et al. (2020) data has a *jump* in figure 5.1. A NFW-fit with just two free parameters (eq. 3.1) might be too rigid to properly reflect on small scale deviations such as an expanded or contracted inner halo. This is especially true since a halo is allowed to be expanded on the inside and contracted at larger radii or the other way around.
The concentration parameter seems unfit to reflect on a cored or steep inner density distribution.

5.3. Dark Matter Surface Density

Σ_{DM} is the dark matter surface density. To calculate it from simulation data I projected the positions of the dark matter particles onto an arbitrary plane (x-y-plane) to mimic observational restraints. The mass within the stellar half-mass radius is then used to calculate the surface density. The total stellar mass in central galaxies was determined by cutting off all particles after 0.1 $\mathrm{R_{vir}}$. The black points in figure 5.3 are Magneticum data from the original sample with 469 halos at redshift zero. Log Σ_{DM} is plotted against

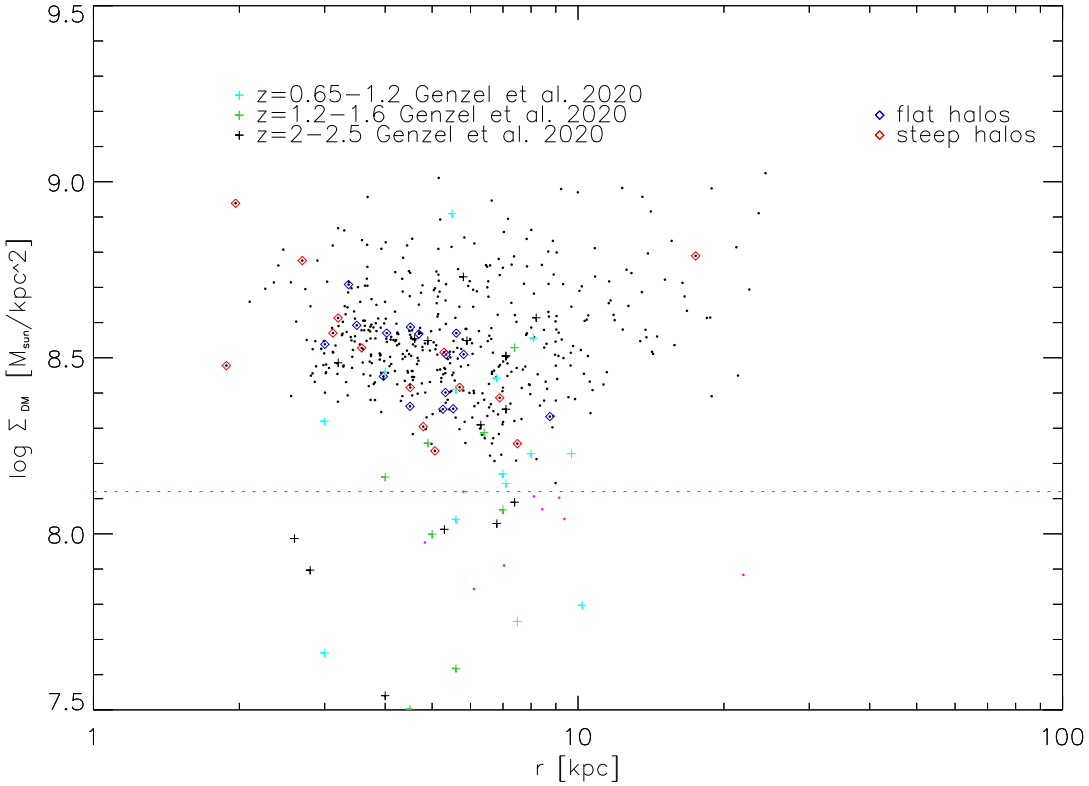

Figure 5.3.: Logarithmic dark matter surface density plotted against the radius within which it was calculated. For The Magneticum data (black and magenta) the stellar half-mass radius $\mathrm{R_{1/2}}$ was used. Genzel et al. (2020) observational data uses the effective radius $\mathrm{R_e}$, which is equivalent to the disk scalelength from Mo et al. (1998, p.321). Magneticum and observations roughly cover the same area, with observations tending towards lower values. Blue and red symbols mark the flat and steep halos from figure 5.1. Unexpectedly both do not show obvious correlations between the inner slope and the dark matter surface density. This also contradicts the proposals of Genzel et al.(2020, p.20). The magenta data was added to the original sample of 469 halos. These halos show a low dark matter surface density (log $\Sigma_{\mathrm{DM}} \leq 8.12$) and are hereby defined as *low density* halos.

the respective half-mass radius within which it was calculated.
Neither the flat nor steep halos from figure 5.1 show clear tendencies in this plot. Again, this is surprising since one would expect a lower dark matter density from a cored halo and a higher one from a steep halo. The average of the logarithmic densities of these two samples are actually identical to the second position after decimal point. It is especially surprising when comparing the radii that are used for calculating the slope and Σ_{DM}. The cores of my flat halos are within one to two percent of $\mathrm{R_{vir}}$. I divided $0.02{\cdot}\mathrm{R_{vir}}$ by the half-mass radius for each flat halo. On average this fraction is 1.10 thus both radii are roughly the same. If Genzel et al. (2020) are right and cores form by expanding dark matter from their inside then we should have seen the flat halos at low values in figure 5.3. Expanding the dark matter from the cored area would remove it from the area within which Σ_{DM} is calculated as well since the radii are similar. From a simulation standpoint I cannot confirm the supposition of Genzel et al. (2020).
When comparing our data to observational data from Genzel et al. (2020) in figure 5.3 keep in mind that they only analysed disk galaxies. They also used the disk scalelength (also effective radius R_e) from Mo, Mao, and White (1998, p.321) as radius for Σ_{DM} and their radii do not cover values above 10 kpc. The observations from the redshift bin closest to zero (z=0.65 to z=1.2) roughly cover the same area as the Magneticum data. The Genzel et al. (2020) sample generally tends towards lower densities. What Magneticum originally did not include are the values at the low end of Σ_{DM} that Genzel et al. (2020) found.

5.4. Low Dark Matter Surface Density Halos

In search for these low surface density halos I examined the halos that were originally excluded through the slope-fit criterion (see appendix). Some of them showed a low dark matter surface density ($\log \Sigma_{DM} \leq 8.12$) and have been added to this and the previous plots retrospectively. They are marked in magenta in figure 5.3, 5.2 and 5.1 and will be labeled *low density* halos. Since the slope-fit criterion biased the sample towards heavier halos with relatively more dark matter particles it is no surprise that low Σ_{DM} halos were missing so far.
So Magneticum does also produce low dark matter surface densities relative to its sample, while not quite reaching the lowest observed values. We have found cored halos as well as low dark matter surface density halos comparable to those of Genzel et al. (2020) within the Magneticum simulation. It is now interesting to trace the properties of these newly added halos.
The first thing that becomes obvious is that the majority of my low density halos have a radius similar to the observations, which is good for comparison. These halos are also at the lower end of stellar masses (fig. 5.2). Furthermore the majority of low density halos tends to populate lower concentration parameters in figure 5.2, with two even being at the bottom end of the whole sample. If this were the result of the halo simply having a lower total DM content than halos of similar size, we would see a normal NFW-fit and c parameter but with lower total density values. But indeed the concentration parameter

changes in comparison to the rest of the sample. It seems like the low concentration parameter could be the result of the same dynamics that also decrease the inner dark matter density. If the low Σ_{DM} values are created by expanding the inner dark matter content then lower c parameters would be a logical consequence. However, with some halos also having larger values, the trend is not as definite as to claim a clear correlation between the two parameters.

I also analysed the inner slope of the low density halos (fig. 5.1). Again, these magenta values have been added to the original sample belated. Since they have only few dark matter particles in their inner part it is no surprise that the linear fits to the logarithmic inner slope were not as good as the rest of the sample. Thus I ran multiple fits and calculated the average (for more information see the appendix). If one looks at figure 5.1 there is no obvious tendency to be seen for the magenta data. The majority scatters closely around -1, which is the expected value for a normal NFW. One halo shows a very steep slope while another one is located at almost zero. I do not find a relation between a low inner dark matter surface density and a cored distribution. Once again this is contradictory to the results of Genzel et al. (2020), which suspect that flat halos relate to low dark matter surface densities. They propose that "[...]dark matter equivalent to 30 ($\pm$ 10)% of the final baryonic bulge mass was removed from the galaxy core during bulge formation "(Genzel et al., 2020, p.20). These halos should then evolve into the cored halo population at lower redshift. But I neither see a tendency of cored halos to have low dark matter surface densities nor do the selected low Σ_{DM} halos show a flat slope.
In summary I find halos with low dark matter surface densities which do not show flat cores but do tend towards lower concentration parameters. A possible explanation for this phenomena could be that they expand their dark matter uniformly within the inner part. Thus lowering their inner density without altering their slope. This suspicion should of course be considered with caution since the correlation is vague and the concentration parameter is not well-suited to describe small scale changes as already pointed out earlier. Their slope values do not seem to reflect on the small dark matter content at all, contradicting assumptions of Genzel et al. (2020).

6. Halo and Parameter Evolution from z=2 to z=0

Several halo properties at redshift zero and their correlation or missing correlation have just been discussed as well as a comparison to observations. I will now show plots that depict the evolution of these halo parameters throughout formation history and differentiate between the three different halo samples. All plots will depict values in dependence on the time from 10.5 Gyr in the past (redshift 2) to the present (redshift 0). Halos within one sample retain the same color for all plots of that sample. If a merger happens in the simulation, the progenitor of a halo is simply determined as the most massive halo prior to the merger.

6.1. Evolution of the Inner Slope

I will open with analysing the change in the inner slope parameter through time. Figure 6.1 depicts this evolution for halos of the flat, steep and low density sample. I used 4 radial bins and the linear fit - as discussed in section 4.2 - to gain the inner slope. The small bin number was necessary mainly because of a lack of dark matter particles at high redshifts. The fitting process for these plots was slightly changed. Instead of making fixed logarithmic bins (let us label this *bin technique*) as for the plots in previous chapters, bins are now set so that the number of particles is distributed equally between them (*particle technique*). Again this was done in the inner one to two percent of the virial radius.
What becomes obvious is that the volatility of the values in each plot is extremely high. Only the black line in figure 6.1 on the top middle plot depicts a relatively smooth evolution. It is the third most massive halo from Magneticum's box4 at z=0 and is actually the BCG (brightest cluster galaxy) of a galaxy cluster. It thus has a large amount of data points and shows significantly less scattering than all other halos.
This scattering also increases with redshift for basically every halo in any sample. This is not surprising since halos gain dark matter through mergers and dark matter particles will be rarer at high redshifts. Thus the scatter of slope values seems to be founded in the lack of dark matter particles and the resulting large error in the fitting process.
In an analogous assertion one could argue that the volatility has a physical origin. More massive halos will be less influenced by events like mergers than small ones, explaining the rather continuous curve of halo 3. At the same time halos towards higher redshifts are less massive and experience more mergers, which could disturb the inner distribution. This would account for the increase in scatter with redshift.

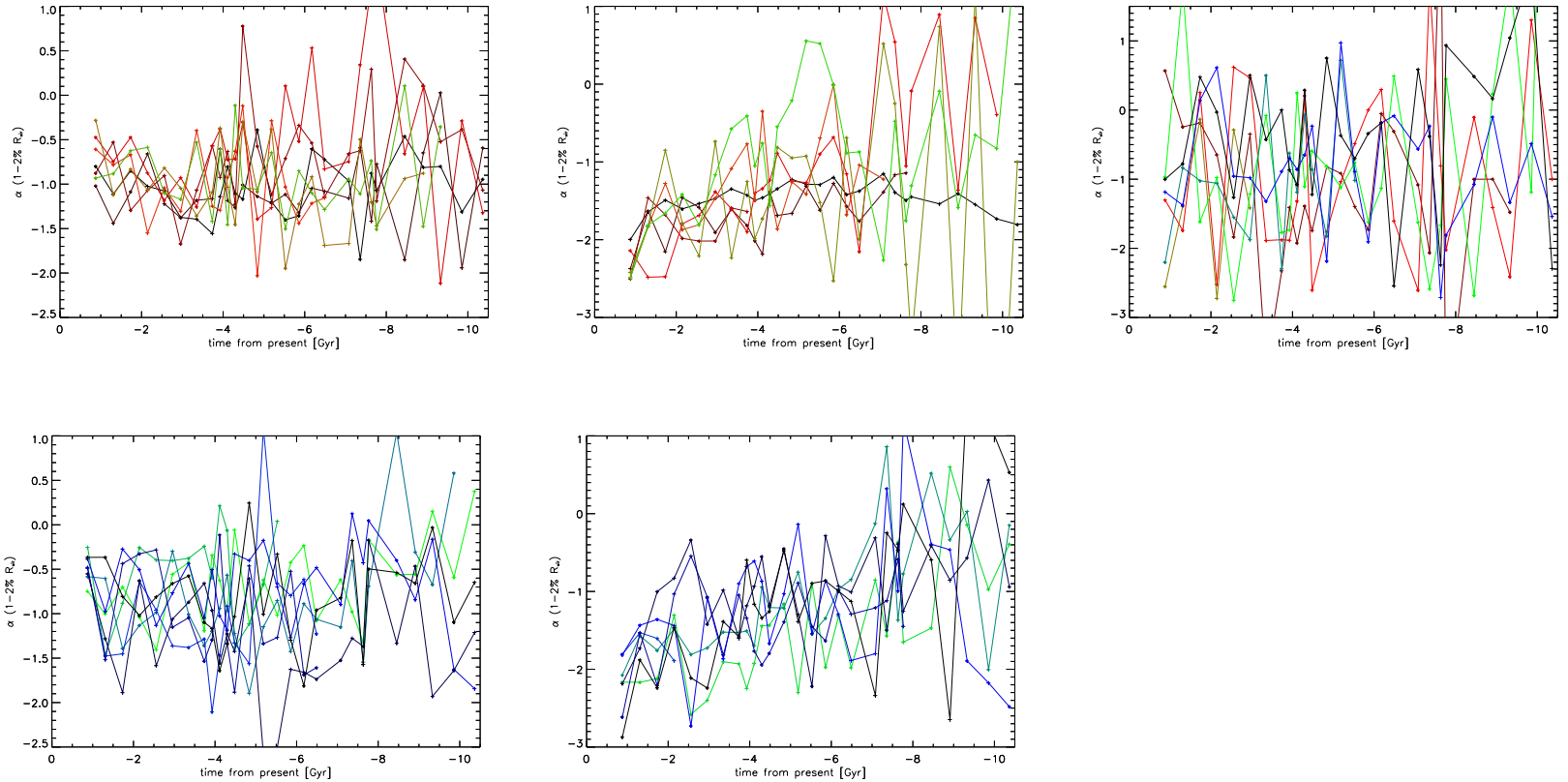

Figure 6.1.: Evolution of the inner slope from -10.5 Gyr (redshift 2) to present (redshift 0). Values are generated from fits to 4 bins with the *particle technique* and are only calculated for central halos, since the virial radius is needed for calculation of α. Left: Values for the flat halo sample are divided into two plots for better visibility. While many halos show an upward trend from -4 Gyr onward the evolution is generally very scattered, especially at high redshift. Middle: Inner slope for the steep sample distributed over two plots as well. Again the change to more negative values takes place after -4 Gyr and volatility increases with redshift. Right: Alpha values for low density halos. Because of few dark matter particles the values scatter throughout the whole formation history.

All these arguments have merit, but I suspect that the lack of data points is the main driver for the high volatility. At this point it also seems uncertain if the slope derived from observations like in Genzel et al. (2020) is a sensible tool to parametrize halos. Verifying parameter evolution with observations is difficult. We cannot know if for example the cored halos from Genzel et al. (2020) in figure 5.1 at z=2-2.5 are really the progenitors of those at z=0.65-1.2. And because of the large scatter in figure 6.1 the simulation can neither make clear statements about the evolution.

Despite all these unfortunate circumstances the plots do carry some information. Firstly the values for each halo sample at redshift zero in figure 6.1 roughly match those derived from the bin technique in section 5.1. Especially the steep halos almost all still lie within the original range between -2 and -3. The slopes of the low density halos remain around -1 and some scattered far above and below. Since the scatter for these halos is large up until z=0, one has to wonder if the assertions from figure 5.1 still hold merit. The standard deviation of the slope values for this sample are not too large. Thus I believe the conclusion that low density halos do not necessarily have flat cores is still true.
For the flat sample in figure 6.1, values at z=0 have slightly decreased in comparison to figure 5.1, somewhat similar to the averages in table I.2. But besides one halo all values are still less negative than -1, most around -0.5. This is reassuring in the sense that the inner slope is relatively consistent for both techniques.
Even tough we cannot quite know what happened before -4 Gyr, we see a trend towards low or high slopes set in afterwards. This equals z=0.35, which is lower than the lowest Genzel et al. (2020) redshift bin. The top plot of the flat sample depicts an average increase in α from roughly -1.2 to -0.7. Similarly the steep halos in the top plot evolve from roughly -1.4 to -2.3 on average. The fact that this is clearer in the top plots might come from more massive halos being shown there.
If one takes a look at figure I.2.1 the density distribution of the cored halos at z=0 really is flat. Assuming the developments from $\alpha \approx$-1 towards the low or high values to be of physical nature, one can formulate some (cautious) conclusions. Whether a halo is steep or flat does not seem to be determined in its early stage, neither do they have unusually high or low values at -4 Gyr, where the scatter becomes less. This would stand in direct contradiction to conclusions made by Genzel et al. (2020, p.20) that core formation happens during the first gas-rich formation phase at high redshift. Then again the Genzel et al. (2020) data only reaches redshift 0.65 at which point the Magneticum scatter in the inner slope is still large. Thus it is not possible to claim that Magneticum even has flat halos at this stage.
There are physical processes that can explain this development for the flat sample. As mentioned in section 5.1 infalling gas-clumps, stellar winds, supernovae and AGN feedback can create cored dark matter distributions. It makes sense that these processes need a certain time to significantly alter the density distribution, although it is curious that the development sets in this late in formation history.
In summary, from a simulation standpoint it seems like the slope of a halo at z=0 is not determined until roughly z=0.35. Unfortunately the volatility of the values is generally

very high. The sensibility of alpha as a halo parameter is put into question. Future research, especially high resolution simulations, will need to investigate due to what and when exactly a halo develops the characteristic of a cored or steep distribution.

6.2. Evolution of the Concentration Parameter

Figure 6.2 shows the evolution of the concentration parameter (top row) and the stellar mass (bottom row) of the respective sample (left: flat; middle: steep; right: low density). Keep in mind that there are different ranges on the y-axis and one logarithmic axis, which was necessary to include all halos in the bottom middle plot. Every halo within one sample has a consistent color. I will now define the names of the colors in the respective sample to be able to refer to each halo in all plots. The colors for the flat sample as seen in the stellar mass plots (fig.6.2 & fig.6.3) at redshift zero from highest to lowest value are: black, brown, turquoise, beige, orange, cyan, black, dark red, blue, olive, lime, light blue, red, navy and dark blue. For the steep sample the sequence in the mass plots at z=2 (-10.5Gyr) is: black, cyan, navy, blue, dark blue, lime, black, brown, green, light blue, red, orange, dark red and beige. Same for the stellar mass plot of the low density sample at z=0: brown, cyan, dark blue, blue, black, beige, lime and red. Unfortunately some colors are quite similar and black occurs twice.
On a first note the majority of halos exhibits a flat and relatively constant curve from z=2 to z=0. The concentration parameters of the flat sample generally evolve from a range of roughly 10-15 to a slightly more spread distribution towards higher values (10-20). The steep sample experiences a minor increase from z=2 to z=0 as well. Unfortunately the low density sample has less halos and they often only become central halos at low redshift, which is necessary for calculating c. Nonetheless most low density halos also feature a rather constant evolution of the concentration parameter. Almost all curves have an up and down scatter of about one to two, which seems to be a little worse at high redshift, where most halos have less dark matter particles.
One can use the stellar-mass plot as indicator for events occurring in the luminous part of the galaxy, such as mergers. From roughly -10.5 Gyr onward the universe was in a phase in which the cosmological structures were forming or had already formed and began to merge with each other, creating larger systems. Thus it is not surprising to see all halos experiencing an effective stellar mass growth throughout formation history. While the flat and low density stellar mass plots look roughly the same, the steep halos actually start off at significantly lower stellar masses of only a few $10^9 M_\odot$.
Is there an interplay between these two parameters? In some cases the concentration parameter seems to react to a rapid increase in stellar mass. The cyan and olive flat halos at high redshift, the dark blue flat halo at -7 Gyr and the red steep halo at almost all times experience a boost of c when m_{star} rises. Unfortunately many halos only become centrals after a big stellar mass gain, thus we cannot analyse the reaction of c to the (suspected) merger event.

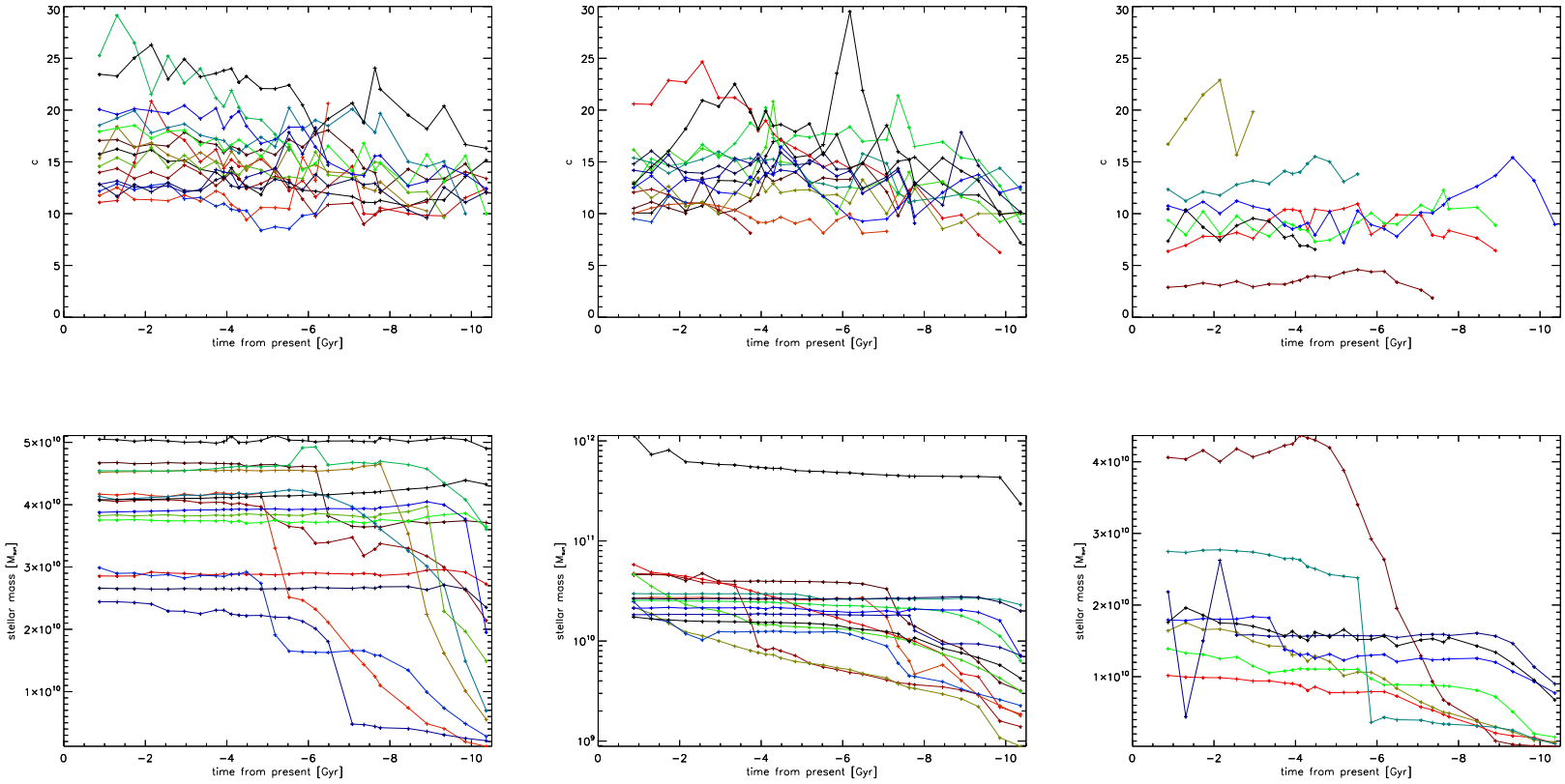

Figure 6.2.: Evolution of concentration parameters (top row) and stellar mass (bottom row) for the flat (left), steep (middle) and low density (right) halo sample. The concentration parameter of all samples is only seldom subject to major changes and evolves quite constantly. Stellar mass increases from z=2 for all halos either smoothly (probably star formation) or rapidly (probably a merger). Some halos show an increase of c with rising stellar mass. But generally there seems to be no relation between the concentration parameter and the stellar mass, nor with the inner slope from figure 6.1.

At the same time many halos depict completely different relations. The concentration parameter of the beige flat halo at high redshift and the blue low density halo at -2.5 Gyr are unperturbed by a significant change in stellar mass. In other cases c exhibits a strong change in value while this is not reflected in the stellar mass evolution. This is true for the blue flat halo at -6.5 Gyr, the turquoise flat halo from -5.5 Gyr onward, the red flat halo at -2 Gyr, the upper black halo in the steep c-plot at -6 Gyr and the beige low density halo at -3 Gyr. These halos either increase, decrease or have a spike in their concentration parameter curve without an indicator of an event happening in the stellar mass plot.
As concluded earlier the inner slope of the flat and steep sample in- or decrease from -4 Gyr onward. This might have an influence on the concentration parameter and would result in a diverging progression between the samples. However, as one can see in figure 6.2 the evolution of the concentration parameter does not seem to differ from one sample to the other, not even after -4 Gyr. The concentration parameter does also not reflect on changes in stellar mass or vice versa. It is obviously very difficult to find a reliable correlation between c and other halo properties.

6.3. Evolution of the Dark Matter Surface Density

As in figure 5.3, I calculated the dark matter surface density for the top row in figure 6.3 by projecting the location of every dark matter particle on the x-y-axis. Σ_{DM} is then equal to $\Sigma \mathrm{m_i}/(\pi \cdot \mathrm{R}_{1/2}^2)$ including all particles within the half-mass radius. The middle row shows the stellar mass as in the previous figure and the bottom row depicts the evolution of $\mathrm{R}_{1/2}$. Be aware of different y-axis ranges and the logarithmic scaling in the middle.
There are trends and correlations to be found here. In almost all cases and for all samples the surface density decreases over time. They all start off at a range of roughly 8.5 to 9 log Σ_{DM}. The flat sample has a few halos above 9 at z=2 and the low density sample is tending towards the lower end of the range. So at z=2 there is already some indication of the low Σ_{DM} values that will form until z=0. After 10.5 Gyr of time at z=0 the majority of flat and steep halos lie in the range of roughly 8.3 to 8.8. As a logical result of the sampling conditions the low density sample shows a lower range of 7.9 to 8.2 at redshift zero. Even though they start off with slightly lower values the difference to the rest of the sample at z=0 is far more significant. The low density sample reduces its dark matter density more than the other halos.

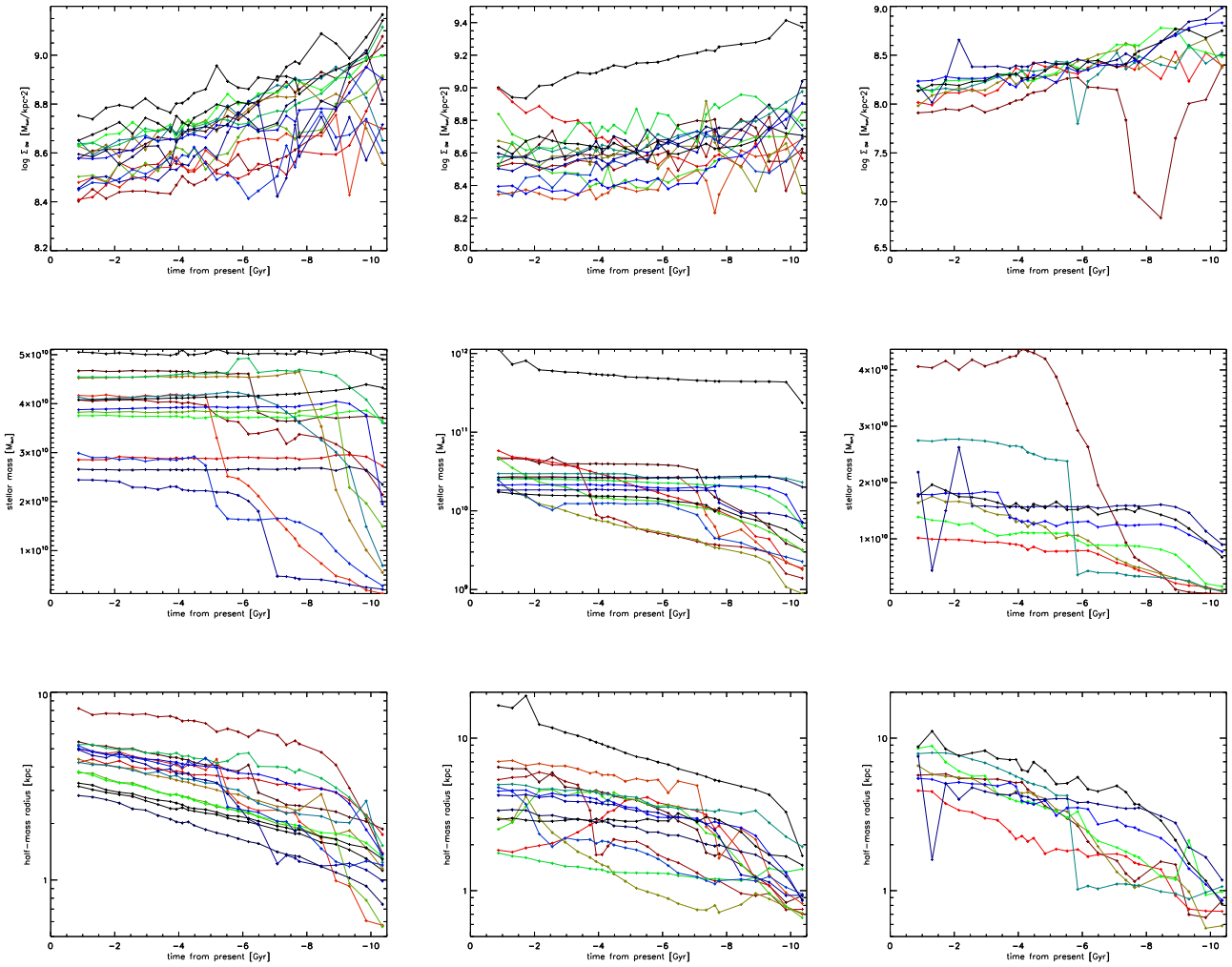

Figure 6.3.: Evolution of dark matter surface density (top row), stellar mass (middle row) and half-mass radius (bottom row) for the flat (left), steep (middle column) and low density (right) halo sample. All samples depict a general decrease of Σ_{DM} over time. Stellar masses mostly rise at high redshift presumably through star formation or mergers. The half-mass radius shows a continuous increase throughout formation history. A quick boost of stellar mass indicates a merger and comes with an increase of Σ_{DM} in the majority of cases. Often the half-mass radius gives a more detailed reflection or even prediction of the DM surface density curve. A decrease of the half-mass radius results in higher Σ_{DM}.

From the middle and bottom row in figure 6.3 one can see the stellar mass and half-mass radius values for the respective samples aligned under each other. In many cases Σ_{DM} increases during phases of stellar mass growth. This behaviour is shown by the cyan and beige flat halos, the light blue steep halo and the lime low density halo, all at high redshift. It also occurs at lower redshifts for the light blue flat halo around -5.5 Gyr and the lime and beige steep halo at roughly -2 Gyr. The stellar mass growth in these cases is mostly a relatively steep and rapid increase. A rapid growth is an indicator for a merger, since mass growth through star formation should be more continuous. The merging halo would not only add stellar mass but also dark matter to the main halo. Thus this correlation with the inner dark matter content is physically sensible.
There are also less swift surges in the stellar component, which do not seem to alter the Σ_{DM} curve visibly. Even tough the turquoise and dark red flat halos increase their stellar mass during the first 2.5 Gyr the dark matter density is falling similar to the general trend and in contrast to the examples mentioned before. The same progression is also true for the blue and dark blue halos in the low density sample at high redshift. These stellar mass growths are not rapid and flatten throughout this period. This supports the assumption of mass growth not through a merger but through star formation, since it shrinks the gas content for star formation itself. Thus if a halo shows a dark matter surface density increase within $R_{1/2}$ contrary to the general downward trend depends on the way the stellar mass grows. A merger will enlarge the dark matter content while continuous growth through star formation does not affect Σ_{DM} significantly. This is very logical since a halo can accumulate new dark matter in a merger, but not through star formation within the halo itself.
However, not all halos follow these correlations. The brown flat halo at -6.5 Gyr, the olive flat halo at -9 Gyr and the dark red steep halo at -4 Gyr have a very rapid growth in stellar mass. Despite this both Σ_{DM} functions show basically no reaction, much less an increase. What makes these halos react differently from the others and the expectations will have to be further examined. The green steep halo also behaves unexpectedly. It features a dark matter boost at high redshift, even though the appearance of the stellar curve indicates mass growth through star formation and not a merger. What also sets this green halo apart from the others is a slightly decreasing half-mass radius, while others increase. One approach of what causes this would be that star formation is concentrated in the inner most part of this galaxy. It would cause stellar mass growth in the depicted way while reducing $R_{1/2}$. Since Σ_{DM} is calculated within the half-mass radius, it might have gotten artificially increased without actual dark matter accretion happening.

As discussed, the mass growth can reflect on the dark matter density growth. But in some cases the half-mass radius actually predicts the Σ_{DM} evolution in more detail. Spikes in the density curve are often preceded by spikes in the half-mass radius. These spikes can be seen from beige (two peaks) and cyan flat halos at high redshift, beige steep halo at -2 Gyr, the lime low density halo at -9.5 Gyr and the beige low density halo at -8.5 Gyr. All of them display stellar mass growth, but not in a way that would reflect on the spiked behaviour of Σ_{DM}. The spike in Σ_{DM} and $R_{1/2}$ are always roughly 0.5 to 1 Gyr apart,

with the change in radius being earlier. Thus a rise and fall of the half-mass radius within a relative short time period acts as a predictor for a similar behaviour for Σ_{DM}.
Yet again four halos react completely different to a rapid stellar mass growth. The steep orange halo around -8 Gyr and the cyan low density halo at -6 Gyr display a rather quick fall and rise (let us call this *dip*) in their dark matter surface density. Massive dips are also found for the dark blue flat halo at -7 Gyr and for the brown low density halo during high redshifts. Again a merger seems to take place for all these halos, which heavily disturbs the inner dark matter content. What makes these halos or mergers different? It seems as though the mergers taking place here are extremely massive and happen to halos that start off rather lightweight. For the brown halo stellar mass growth is large as well, but stretched over a longer period than the dip is visible. The dark matter component might have merged earlier or faster than the stellar component, explaining the delay.
These dynamics can be well-explained with physical processes. From the data one can assume that the two (or more) halos involved in these (major) mergers had similar masses. Thus the gravitational pull from one to the other is more relevant and influential in these cases. At the beginning of the merger one halo pulls dark matter out of the center of the other and thus creates the rapidly decreasing curve. After that the galaxies merge completely and the inner dark matter content is restored or increased, explaining the rise of the curve.

I also want to mention three halos that depict interesting and somewhat particular evolutions. All three are from the steep halo sample. The red, lime and beige halo all feature a steady stellar mass growth during their whole formation history, resulting in a large total mass difference of $5.8 \cdot 10^{10} M_\odot$, $4.2 \cdot 10^{10} M_\odot$ and $1.9 \cdot 10^{10} M_\odot$ respectively. The ongoing growth at low redshift is rather uncommon. These growths do not flatten neither do they indicate large mergers happening. One speculation would be that these halos experience a constant supply of new gas for star formation or multiple small mergers. The dark matter progression for these halos is normal at first. Starting at -6 Gyr the DM surface density of the red halo rises steadily until redshift zero. The same goes for the green halo at -4 Gyr (steep increase from -2 Gyr) and the beige at -2 Gyr. This does not seem to be correlated to the stellar mass function. But what is really interesting is the half-mass radius of these halos. All three depict a rapidly decreasing half-mass radius at the points where Σ_{DM} increases. No other halo, not even from other samples have this trend at low redshifts. Similar to some of the examples before, $R_{1/2}$ seems to be a way better indicator for what is happening with the dark matter surface density. And analogously the development of all three parameters could be explained by a constant star formation in the center, reducing $R_{1/2}$ and somewhat artificially increasing Σ_{DM}. It makes sense that exactly these halos increase Σ_{DM} with smaller radii, since the steep halos are *cuspier* than a normal NFW. If we assume this correlation to be generally true, then the overall trend of falling Σ_{DM} could simply be the result of the rising half-mass radii. Since this is only an educated guess it will have to be further investigated what physics are really at play here.
I would also like to direct attention to the dark blue curve on the right side of figure 6.3.

It is the only halo to have a wide scatter of Σ_{DM} at such low redshift. The upward spike followed by a dip is also reflected in the stellar-mass and only partly in the half-mass radius. One source of this behaviour might be a satellite galaxy passing through the center the halo without merging. This would result in a preliminary rise of inner dark matter content. After having passed the center the satellite would pull dark matter from the large halo and subsequently decrease Σ_{DM}.

Finally I would like to discuss if Σ_{DM} correlates with the other parameters, c or α. Dark matter surface density and concentration parameter both have their general trends. Deviations from this trend like a significantly increasing concentration parameter of the turquoise flat or the red steep halo do not affect their Σ_{DM} value. Neither does a rapid decrease of c affect the dark matter surface density of the red and orange flat halo or a spike in the black steep concentration parameter. Uncommon structures as a dip in the dark matter density of the dark blue flat halo or a large up and down movement of the dark blue low density halo are also not reflected in the concentration parameter.
Since the inner slope has such a high volatility it is not possible to find detailed relations. However, as we established the development of a cored or steep halo supposedly does not set in until -4 Gyr. At the same time the evolution of the flat and steep dark matter surface density has a steady trend from z=2 onward. This trend does not change when the cores or cusps are formed. The process that creates the deviations in the slope do not seem to affect Σ_{DM} in a relevant fashion, as was also suspected in section 5.3. This contradicts the interrelationship proposed by Genzel et al. (2020), whereby the core was created through expanding inner dark matter equivalent to 30% of the final bulge mass. The loss of dark matter density of halos that do form cores is basically identical to the loss of steep halos in Magneticum. They also do not differ significantly in their final stellar mass. So from a simulation point of view developing a core does not mean loosing a larger part of dark matter within $\mathrm{R}_{1/2}$ than other halos.

In summary many features of the dark matter surface density correlate with the stellar mass and the half-mass radius. The vast majority of halos that experience a large and rapid mass growth, indicating a merger, also see an increase in Σ_{DM}. In contrast a smooth and flattening mass curve leads to a normal slowly decreasing density in most cases and can probably be lead back to star formation without mergers. For many halos the half-mass radius actually gives a more detailed reflection or even a forecast for the behavior of the dark matter density such as spikes or an uncommon Σ_{DM} increase at low redshift. It will have to be determined if a shrinking half-mass radius overestimates dark matter accretion artificially. These correlations give valuable insight into the evolution of dark matter halos, however, they are surely inadequate to include all physics at play, which is why some halos show different behavior. I cannot confirm that cored halos expanded a significant part of their dark matter content during formation. It will be very interesting to use zoom-in simulations with higher resolutions to get a better understanding of the evolution of the inner slope.

7. Dark Matter Surface Density at Redshift Two

After I have discussed various halo properties at redshift zero and their evolution I will now give a more detailed insight into the dark matter surface density at redshift two.

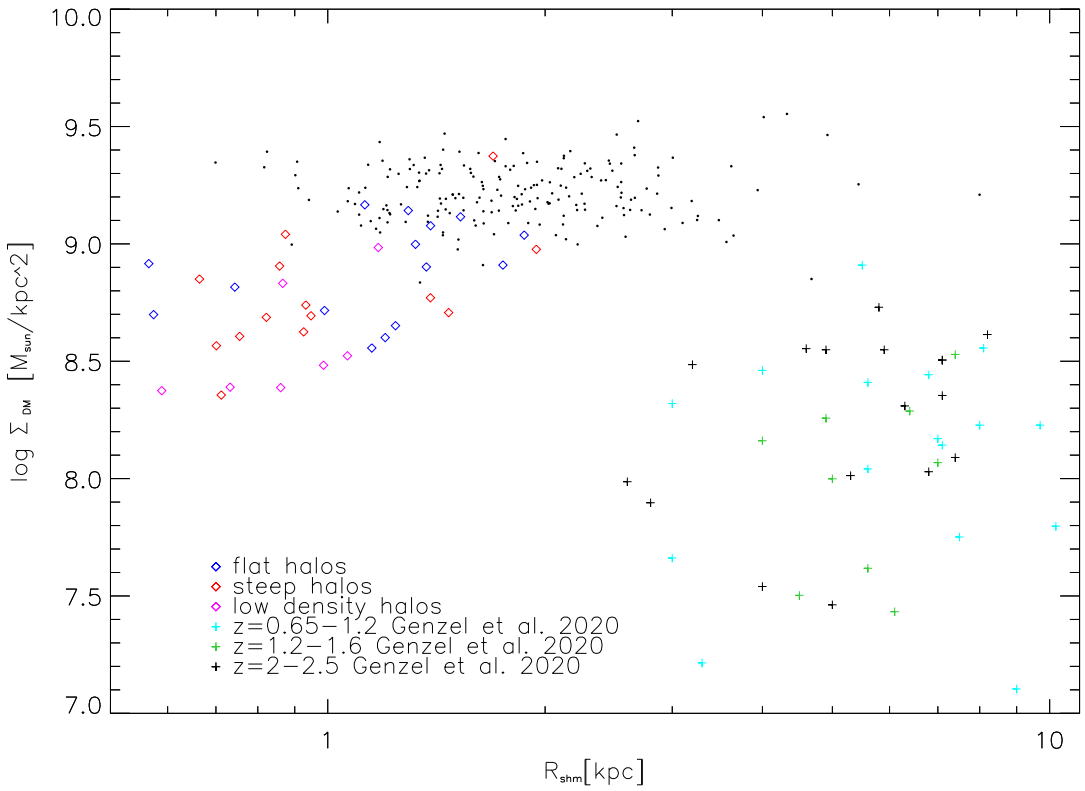

Figure 7.1.: Dark matter surface density plotted against the radii within which it was calculated. Black points are Magneticum data from the 201 most massive halos at z=2. Colored diamonds depict log Σ_{DM} at z=2 from the samples defined in section 5. Most of them differ in radius and density values, which might originate from them being less massive. All three redshift bins from Genzel et al. (2020) observational data diverge significantly from Magneticum data. Even though the smaller radii of the simulation data might give some explanation for the Σ_{DM} offset, it is unclear why both disagree this much.

The black points in figure 7.1 are Magneticum data from the 201 most massive halos at z=2. Blue, red and magenta diamonds mark the Σ_{DM} values at z=2 from the respective samples defined in section 5. Only few of the halos from the black data and the three samples overlap. This is not surprising since only two halos from all three samples are within the 201 most massive halos at z=0. The three colored samples tend towards lower radii and lower Σ_{DM}. This could simply be the result of them being less massive than the black halos. On the other hand it is surprising since we have found out in section 6.3 that Σ_{DM} usually increases with lower radii.

The data from Genzel et al. (2020) completely disagrees with the simulation data. Independently of the redshift bin, all observations populate higher radii and have less dark matter surface density than the black Magneticum halos. Only the Σ_{DM} values from the three samples somewhat match their data, but at completely different radii. It is very curious how the z=0 Magneticum data fits the observations very well, but is completely off at higher redshift. The Genzel et al. (2020) data itself seems to only slighly decrease throughout time.
As already once pointed out they use a different definition for within which radius they calculate Σ_{DM}. Some halos from section 6.3 supposedly increased their dark matter surface density by decreasing the half-mass radius. The offset in this plot could have the same origin. The red steep halo in figure 6.3 for example develops from log Σ_{DM}= 8.6 to 9 while the radius reduces from 4 kpc to 2 kpc. Let us set the average of the observational data in figure 7.1 at log Σ_{DM}=8.3 and r=6 kpc as well as the black Magneticum data to log Σ_{DM}=9.2 and r=2 kpc. One can transpose the change that the red steep halo exhibits to the change of these two samples (black Magneticum and observations). On a non-logarithmic scale the increase of surface density for the red halo from figure .6.3 is $6{\cdot}10^8 \mathrm{M}_\odot/\mathrm{kpc}^3$ for Δr=2 kpc. This would account for $9{\cdot}10^9 \mathrm{M}_\odot/\mathrm{kpc}^3$ of the actual $1.39{\cdot}10^8 \mathrm{M}_\odot/\mathrm{kpc}^3$ that Magneticum is above the observations. Of course the development of the red halo was within the same halo, whereas I just looked at multiple halos. But I explicitly checked that both samples populate similar ranges of total stellar mass and are thus comparable. All this does not justify the whole offset and is only an estimate but it gives some explanation for why the data is so different. What is still unclear is why Magneticum has so much lower radii at z=2 in the first place, even though the masses are similar. One reason could be the different definitions that were used for the radii.
In short, the samples of interest from redshift zero now neither overlap with the most massive halo data from Magneticum, nor the observational data. Genzel et al. (2020) depict lower Σ_{DM} values while having larger radii. Even though there are some explanations for this it will be important to investigate what exactly causes this disparity of simulation and observation.

8. Conclusion

In this work I have presented data and results drawn from the Magneticum simulation. I analyzed the inner slope (α) of the inner dark matter component in galaxies at redshift zero and compared it to observations. The halos that showed a slope that was higher or lower than the majority of the sample and the expectation of a NFW-profile were put into separate samples. A cored halos has a less negative slope, while a cuspy halo has a more negative one. The concentration parameter (c) and inner dark matter surface density (Σ_{DM}) of those samples was analysed together with the rest of the 601 most massive Magneticum halos. I also found halos that feature a low dark matter surface density - like the ones observers see - outside of the original sample. I then traced back the properties of these newly added halos.
In the next step I evaluated the evolution of halos throughout their formation history from 10.5 Gyr in the past (z=2) to the present (z=0). I did this for the halos that depicted a flat or steep inner slope and those with low surface density. I traced the development of the inner slope, the concentration parameter, the dark matter surface density, the stellar mass ($\mathrm{m_{star}}$), the half-mass radius ($\mathrm{R_{1/2}}$) and the virial radius ($\mathrm{R_{vir}}$) for these halos.
Lastly I took a more detailed look on the dark matter surface density at redshift two. I compared the 201 most massive halos at this time to the three colored samples mentioned before and observations. From all of these investigations I inferred following conclusions:

- In contrast to other simulations, Magneticum yields dark matter cores similar to observations. It also includes halos with a significantly steeper slope than a perfect NFW-profile would have. Since the flat halos presumably deposited dark matter from their core towards the outside, one would expect them to have expanded dark matter distributions on the inside and the steep halos vice versa. However, the cored halos do not tend towards lower concentration parameters or lower Σ_{DM} values. Neither do the steep ones tend towards higher values. This stands in contrast to conclusions made by Genzel et al. (2020), which state that a core is formed by expanding dark matter equivalent to 30% of the final bulge mass.

- The simulation also covers halos that have a dark matter surface density significantly lower than the majority of halos. They also lie in the same range as the observations. These low density halos lean towards lower concentration parameters, indicating an expanded inner dark matter distribution. At the same time they do not feature a core, when looking at their inner slope values. This is again contradictory to the assumptions of Genzel et al. (2020) that cores and low dark matter surface densities relate to each other.

- The evolution of the slope parameter has very high volatility, mainly due to a lack of resolution. It is not possible to make conclusive statements for any of the three samples (flat,steep and low surface density) from -10.5 Gyr to -4 Gyr from the present. At z=0.35 (-4 Gyr) the scatter decreases for the flat and steep sample. At this point these samples show rather normal slope values around -1. They then evolve to their distinct high or low values at z=0. In contrast Genzel et al. (2020) assume that cores were created at high redshift during the formation of the galaxy bulge. Unfortunately I cannot make statements about the slope above z=0.35 which is lower than the lowest redshift bin from Genzel et al. (2020). The high volatility and disagreement of simulation and observations calls for a more detailed analysis in for example high resolution zoom-in simulations.

- The concentration parameters of all three samples stay quite constant all the way from z=2 to z=0. They have a relatively small scatter and do not show differences between the distinct halo samples. There is no correlation between c and α to be found.

- The dark matter surface density features a steady decrease from z=2 to z=0. All halo samples roughly start off within the same range. The low density sample reduces its Σ_{DM} parameter stronger than the other two. In accordance with my findings at z=0, but in contrast to the assumptions of Genzel et al. (2020) that I already mentioned, the flat and steep halos do not diverge in their Σ_{DM} evolution. The flat halos do not seem to loose more dark matter within the half-mass radius than the steep ones during the formation of the core.

- The dark matter surface density does also not correlate to the concentration parameter. However, all halo samples depict interrelationships with the stellar mass and half-mass radius. A rapid stellar mass increase indicating a merger also boosts Σ_{DM}. A smooth and flattening rise in $\mathrm{m_{star}}$ implies star formation and does not affect the surface density. This is physically plausible since a halo can only accrete new dark matter in a merger. The half-mass radius often gives a more detailed reflection of Σ_{DM}. A spike in $\mathrm{R_{1/2}}$ precedes a spike in dark matter surface density by roughly 0.5 Gyr to 1 Gyr. A decreasing half-mass radius seems to increase Σ_{DM}. It will be important to further investigate if such changes artificially raise the dark matter surface density and give a false impression of an increased DM content.

- The flat, steep and low density halos populate lower Σ_{DM} and $\mathrm{R_{1/2}}$ values than the 201 heaviest halos at z=2 (black data in figure 7.1). There is also a large offset between those 201 halos and the observational data from Genzel et al. (2020), which have larger radii and lower surface densities. I transposed the correlation of one halo that increased its Σ_{DM} parameter with lower radii during its evolution. This then accounted for most of the offset between the black Magneticum data and the observations, which populate similar stellar masses. It remains unclear why the Magneticum halos have lower half-mass radii at z=2 even tough they have the same masses and align with observations at z=0.

This work was mostly a phenomenological analysis of the properties and evolutions of halos within the Magneticum simulation. I compared my results with observations and gave first suppositions for the physical backgrounds that cause the correlations, missing correlations and evolution of these halos. The Magneticum simulation shows great potential to provide a counterpart to observations where other simulations fail to produce for example cored halo structures. I hope this acts as a stepping stone for further investigations into the subjects of this work. Future high-resolution zoom-in simulations will hopefully give insight into the questions that are left to be answered.

I. Appendix

I.1. Halo Criteria for the z=0 Sample

At redshift zero SubFind finds a total of 148471 main halos in Magneticum. For the a preliminary set of halos I selected the heaviest 601 halos. This ensures that one percent of the virial radius does not fall below the gravitational softening length. Latter is set at 1 kpc for stars and 2 kpc for gas and DM. The sample's value for one percent of R_{vir} ranges from 1.9 kpc to 16 kpc with an average of 3.68 kpc. Furthermore I reduced the sample by looking at the data from the inner log ρ- log r plots, which create figure 5.1. Halos for which the number of dark matter particles within a radial bin fell below 18 more than twice were taken out of the sample. This ensures that the density values from each bin are calculated with a statistically sufficient number of particles. For information on the used number of bins see table I.1. Very few halos were omitted from individually looking at their inner density distribution, which was so scattered that no sensible linear fit could have been applied. These criteria reduced the sample to 469 halos, which I call the *original* sample within the work.

Halo index	Number of bins
0-200	19
201-300	9
301-400	7
401-600	6

Table I.1.: Number of bins used in the inner slope fit to the DM density between one and two percent of the virial radius at z=0. The numbers are set to maximize the data points to which I can fit while keeping statistically enough particles within each bin.

I.2. Flat Halos at z=0

The halos with a flat ($\alpha \geq -0.6$) inner slope derived from figure 5.1 are a very important part of this work. Thus it is important to make sure these halos indeed show this feature. For this I refitted the 15 halos from the sample with changing number of bins from 4 to (including) 8. For visualization, one linear fit to the log ρ-log r plane for each halo can be seen in figure I.2.1. Mind that the depicted number of bins does not necessarily match those from which the values in figure 5.1 were derived. What one can see is that

the data points are clearly aligned quite flat and the halos do really have a cored density distribution.
Table I.2 shows that for some halos the average of these multiple fits is above the value from figure 5.1. Taking the average and the worst-case standard deviation for α within each halo into account, many halos would fall out of the original definition of the sample. Of course this also leads to the apprehension that some halos with slopes slightly below -0.6 are wrongly missing in the sample.
Thus the absolute values from figure 5.1 should be regarded with caution. However, I conclude they are sufficient for the classification of the flat halo sample, since every halo is still considerably flatter than the NFW. Hence the sample was kept as seen in table I.2.

Halo index	Slope in plot	Average	Standard deviation
276	-0.592	-0.589	0.0884
389	-0.596	-0.635	0.0489
406	-0.546	-0.705	0.114
423	-0.318	-0.274	0.0538
430	-0.501	-0.444	0.0407
433	-0.463	-0.399	0.0631
448	-0.571	-0.580	0.0624
463	-0.590	-0.572	0.0747
464	-0.298	-0.416	0.109
488	-0.569	-0.661	0.0940
503	-0.575	-0.653	0.050
527	-0.273	-0.293	0.0411
536	-0.382	-0.547	0.137
559	-0.594	-0.592	0.0280
594	-0.414	-0.521	0.0664

Table I.2.: Table containing the value for α from figure 5.1, the average from fits to changing bin numbers from 4 to (including) 8, and the standard deviation for each flat halo at z=0. The average value is often higher than from figure 5.1, where the flat sample was defined. Despite this I conclude that the original sampling from figure 5.1 is still valid.

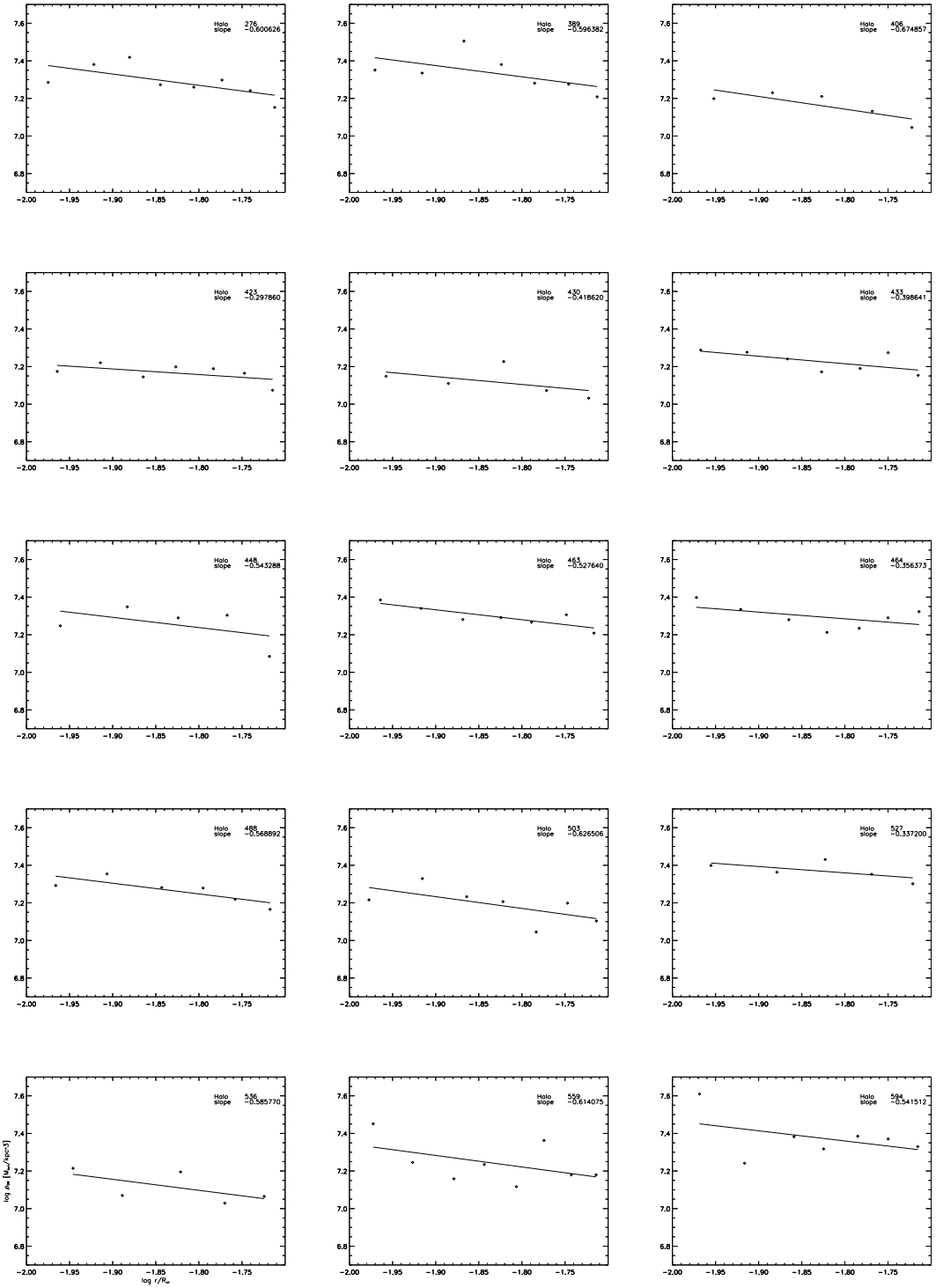

Figure I.2.1.: Double logarithmic plots with dark matter density plotted against r/R_{vir} within one to two percent of R_{vir}. The black line is the least squares fit from equation 4.3. The depicted number of bins in each plot do not necessarily match those from which the values in figure 5.1 were derived. Halos show a clear flat/cored density distribution.

I.3. The Slope of Low Σ_{DM} Halos at z=0

Table I.3 depicts the average inner slope values of the low density sample at redshift zero. They are identical to the values shown in figure 5.1. These halos have especially few dark matter particles to use for the fit. That only allowed for sensible fits to 3,4 and 5 radial bins for fitting. Thus the absolute values should be considered with caution. What can still be inferred is that the low density sample does not show a tendency towards less negative slopes. This is surprising since one would expect the low dark matter density halos to have expanded DM from their center and thus have a cored distribution.

Halo index	Average	Standard deviation
130	-0.76	0.09
298	-0.012	-
424	-1.18	0.27
471	-2.97	0.67
492	-1.019	0.031
542	-1.44	0.06
557	-0.99	0.24
564	-1.19	0.11
569	-0.91	0.20

Table I.3.: Table containing the average (identical to values in fig. 5.1) inner slope values for the low density sample at z=0. Standard deviations are calculated from fit-values using bin numbers 4,5 and 6 per halo. Halo 298's dark matter content only allowed for a sensible fit with 4 and 5 bins.

I.4. Additional Plots

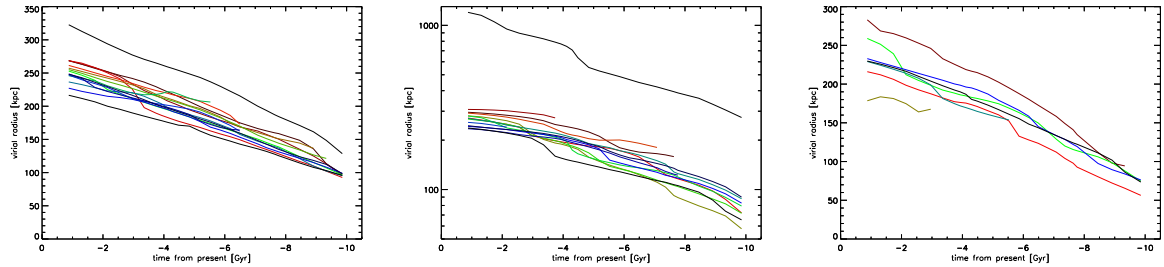

Figure I.4.2.: Evolution of the virial radii from -10.5Gyr (redshift 2) to the present (redshift 0). Values of all halo samples are continuous and show a steady increase towards lower redshift. This makes sense since halos grow through mergers over time. It also confirms that the volatility of the inner slope or the concentration values, which need Rvir to be calculated, do not originate from scattering of the virial radius. Left: flat halos. Middle: steep halos. Right: low density halos.

II. References

Beck, A. M., Murante, G., Arth, A., Remus, R.-S., Teklu, A. F., Donnert, J. M., ... others (2016). An improved sph scheme for cosmological simulations. *Monthly Notices of the Royal Astronomical Society*, *455*(2), 2110–2130.

Brouwer, M. M., Visser, M. R., Dvornik, A., Hoekstra, H., Kuijken, K., Valentijn, E. A., ... others (2017). First test of verlinde's theory of emergent gravity using weak gravitational lensing measurements. *Monthly Notices of the Royal Astronomical Society*, *466*(3), 2547–2559.

Cole, D. R., Dehnen, W., & Wilkinson, M. I. (2011). Weakening dark matter cusps by clumpy baryonic infall. *Monthly Notices of the Royal Astronomical Society*, *416*(2), 1118–1134.

Dekel, A., Ishai, G., Dutton, A. A., & Maccio, A. V. (2017). Dark-matter halo profiles of a general cusp/core with analytic velocity and potential. *Monthly Notices of the Royal Astronomical Society*, *468*(1), 1005–1022.

Di Matteo, T., Springel, V., & Hernquist, L. (2005). Energy input from quasars regulates the growth and activity of black holes and their host galaxies. *nature*, *433*(7026), 604–607.

Dolag, K., & Stasyszyn, F. (2009). An mhd gadget for cosmological simulations. *Monthly Notices of the Royal Astronomical Society*, *398*(4), 1678–1697.

Dolag, K., Vazza, F., Brunetti, G., & Tormen, G. (2005). Turbulent gas motions in galaxy cluster simulations: the role of smoothed particle hydrodynamics viscosity. *Monthly Notices of the Royal Astronomical Society*, *364*(3), 753–772.

Donnert, J., Dolag, K., Brunetti, G., & Cassano, R. (2013). Rise and fall of radio haloes in simulated merging galaxy clusters. *Monthly Notices of the Royal Astronomical Society*, *429*(4), 3564–3569.

Dutton, A. A., Macciò, A. V., Dekel, A., Wang, L., Stinson, G., Obreja, A., ... Kang, X. (2016). Nihao ix: the role of gas inflows and outflows in driving the contraction and expansion of cold dark matter haloes. *Monthly Notices of the Royal Astronomical Society*, *461*(3), 2658–2675.

Fabjan, D., Borgani, S., Tornatore, L., Saro, A., Murante, G., & Dolag, K. (2010). Simulating the effect of active galactic nuclei feedback on the metal enrichment of galaxy clusters. *Monthly Notices of the Royal Astronomical Society*, *401*(3), 1670–1690.

Genzel, R., Price, S., Übler, H., Schreiber, N., Shimizu, T., Tacconi, L., ... others (2020). Rotation curves in z˜ 1-2 star-forming disks: Evidence for cored dark matter distributions. *arXiv preprint arXiv:2006.03046*.

Georgi, H., & Glashow, S. L. (1974). Unity of all elementary-particle forces. *Physical Review Letters*, *32*(8), 438.

Jubelgas, M., Springel, V., & Dolag, K. (2004). Thermal conduction in cosmological sph simulations. *Monthly Notices of the Royal Astronomical Society*, *351*(2), 423–435.

Kapteyn, J. C. (1922). First attempt at a theory of the arrangement and motion of the sidereal system. *The Astrophysical Journal*, *55*, 302.

Larson, D., Dunkley, J., Hinshaw, G., Komatsu, E., Nolta, M., Bennett, C., ... others (2011). Seven-year wilkinson microwave anisotropy probe (wmap*) observations: power spectra and wmap-derived parameters. *The Astrophysical Journal Supplement Series*, *192*(2), 16.

Macciò, A. V., Crespi, S., Blank, M., & Kang, X. (2020). Nihao–xxiii. dark matter density shaped by black hole feedback. *Monthly Notices of the Royal Astronomical Society: Letters*, *495*(1), L46–L50.

Mandelbaum, R., Seljak, U., & Hirata, C. M. (2008). A halo mass—concentration relation from weak lensing. *Journal of Cosmology and Astroparticle Physics*, *2008*(08), 006.

Mo, H., Mao, S., & White, S. D. (1998). The formation of galactic discs. *Monthly Notices of the Royal Astronomical Society*, *295*(2), 319–336.

Mo, H., Van den Bosch, F., & White, S. (2010). *Galaxy formation and evolution*. Cambridge University Press.

Mukhanov, V. F. (2016, oct). Quantum universe. *Physics-Uspekhi*, *59*(10), 1021–1027. Retrieved from `https://doi.org/10.3367%2Fufne.2016.07.037857` doi: 10.3367/ufne.2016.07.037857

Mukhanov, V. F., & Chibisov, G. (1981). Quantum fluctuations and a nonsingular universe. *JETP Lett.*, *33*, 532–535.

Navarro, J. F., Frenk, C. S., & White, S. D. M. (1996, May). The structure of cold dark matter halos. *The Astrophysical Journal*, *462*, 563. Retrieved from `http://dx.doi.org/10.1086/177173` doi: 10.1086/177173

Pontzen, A., & Governato, F. (2012). How supernova feedback turns dark matter cusps into cores. *Monthly Notices of the Royal Astronomical Society*, *421*(4), 3464–3471.

Pontzen, A., & Governato, F. (2014). Cold dark matter heats up. *Nature*, *506*(7487), 171–178.

Springel, V., Di Matteo, T., & Hernquist, L. (2005). Modelling feedback from stars and black holes in galaxy mergers. *Monthly Notices of the Royal Astronomical Society*, *361*(3), 776–794.

Springel, V., & Hernquist, L. (2003). Cosmological smoothed particle hydrodynamics simulations: a hybrid multiphase model for star formation. *Monthly Notices of the Royal Astronomical Society*, *339*(2), 289–311.

Teklu, A. F., Remus, R.-S., Dolag, K., Beck, A. M., Burkert, A., Schmidt, A. S., ... Steinborn, L. K. (2015). Connecting angular momentum and galactic dynamics: the complex interplay between spin, mass, and morphology. *The Astrophysical Journal*, *812*(1), 29.

Tornatore, L., Borgani, S., Dolag, K., & Matteucci, F. (2007). Chemical enrichment of galaxy clusters from hydrodynamical simulations. *Monthly Notices of the Royal*

Astronomical Society, *382*(3), 1050–1072.

Wiersma, R. P., Schaye, J., & Smith, B. D. (2009). The effect of photoionization on the cooling rates of enriched, astrophysical plasmas. *Monthly Notices of the Royal Astronomical Society*, *393*(1), 99–107.

Zwicky, F. (1933). Die rotverschiebung von extragalaktischen nebeln. *Helvetica physica acta*, *6*, 110–127.

III. Acknowledgements

Ich möchte mich von ganzem Herzen bei meinen Betreuern Klaus und Rhea bedanken. Die Kriese hat leider ein persönliches zusammen Arbeiten verhindert. Trotzdem haben sie sich wundervoll um mich gekümmert. Aus jeder Frage und jedem Problem ist ein interessantes und lehrreiches Gespräch geworden. Ich bin sehr froh, dass die beiden schon als ich noch ihre Vorlesung besucht habe, ihr Vertrauen in mich gesteckt haben. Es war mir eine Ehre mit zwei so genialen Wissenschaftern zusammen arbeiten zu können und einen kleinen Beitrag zur Forschung des Teams leisten zu können.
Rhea, Klaus und der Rest des Teams von CAST haben mich sofort in die regelmäßigen Meetings involviert und ich habe mich gleich wohl gefühlt in der Gruppe. Danke an das ganze Team für die schöne Zeit und für die Hilfe bei diversen coding Problemen.
Vielen Dank auch an Tadziu, der sich um meinen Zugang zum System gekümmert hat und ohne den ich die exakten beobachtungs Daten nicht verfügbar gehabt hätte.

IV. Declaration of Authorship

Hiermit erkläre ich, die vorliegende Arbeit selbständig verfasst zu haben und keine anderen als die in der Arbeit angegebenen Quellen und Hilfsmittel benutzt zu haben.

München, den

Unterschrift: